Geol. Mag. **152** (*1*), *2015, pp. 143–165.* © *Cambridge University Press 2014*
doi:10.1017/S0016756814000016

Record of climatic fluctuations and high pH weathering conditions in a thick Ordovician palaeosol developed in rhyolite of the Dunn Point Formation, Arisaig, Nova Scotia, Canada

P. JUTRAS†, M. J. LEFORTE & J. J. HANLEY

Department of Geology, Saint Mary's University, Halifax, Nova Scotia, B3H 3C3, Canada

(*Received* 3 October 2013; *accepted* 13 January 2014; *first published online* 27 May 2014)

Abstract – A thick Ordovician intra-rhyolitic palaeosol was studied to investigate the peculiarities of early Palaeozoic continental environments, shortly before the development of vascular plants, and to compare its pedogenic patterns with those of previously studied intra-basaltic profiles from the same succession. Well-defined K-eluviation from the top of the palaeosol is proportionally met by K-illuviation at the base of the profile, a pedogenic behaviour that was masked in the underlying intra-basaltic profiles due to subsequent eodiagenetic K-enrichment associated with rhyolite emplacement. Greater stability of K (and eventually Mg) than Si in the intra-rhyolitic profile suggests high pH soil water at the time of pedogenesis despite the low base contents of the acidic host rock, and despite evidence for humid weathering conditions. We also observe that, at the base and at the top of the profile, Al_2O_3/Zr ratios are substantially lower than those of the host rock, suggesting Al-leaching and therefore extreme weathering conditions, whereas the middle portion of the profile shows Al_2O_3/Zr ratios that are similar to those of the host rock, suggesting Al stability and therefore less extreme conditions. We interpret these variations in Al_2O_3/Zr ratios as signatures of a cyclic change from sub-humid periods during which Al was stable throughout the profile, to more humid periods with a well-defined seasonality, during which only the juvenile zone of weathering at the base of the profile could have developed sufficiently high pH during dry seasons for Al to be leached, leaving the Al_2O_3/Zr signatures from previous stages untouched higher in the profile.

Keywords: intra-rhyolitic palaeosol, Ordovician, pedogenesis, element mobility, eluviation–illuviation patterns, palaeoclimate signatures, alkaline soil water.

1. Introduction

Insights into Ordovician continental environments have been provided by the study of intra-basaltic palaeosols of the Dunn Point Formation in eastern Canada (Fig. 1a) (Boucot *et al.* 1974; Feakes, Holland & Zbinden, 1989; Jutras, Quillan & LeForte, 2009; Jutras *et al.* 2012), which is part of a volcanic succession that hosts the youngest known palaeosols to have affected primary rocks prior to the Silurian radiation of vascular land plants. Although the intra-basaltic palaeosols were briefly compared with a recently identified intra-rhyolitic palaeosol in the same bimodal succession (Jutras, Quillan & LeForte, 2009), a detailed study of the latter was lacking until now.

Previous studies have suggested that, despite warm and humid climatic conditions, the underlying intra-basaltic weathering profiles evolved in high pH soil water conditions (up to above 8) due to a low production of organic acids by the primitive Ordovician plant cover, which was insufficient to counteract the alkalinizing effect of the mineral–water interactions that take place is soils (Jutras, Quillan & LeForte, 2009; Jutras *et al.* 2012). These authors also argued that rain water pH must have gradually increased during geological times along with the gradual storage of atmospheric carbon in carbonate rocks (Kasting, 1993), making the pre-Silurian portion of the Palaeozoic most prone to developing high pH groundwater conditions, which is also suggested by studies on the K-feldspar (Basu, 1981) and detrital illite (Weaver, 1967) contents of clastic rocks from that period. One purpose of the present study is to compare pedogenic dynamics in acidic versus basic rocks under presumably similar climatic conditions, and to further investigate the peculiarities of weathering processes in alkalinity-prone, early Palaeozoic continental environments. To help distinguish early from late pedogenic features, a thick and mature intra-rhyolitic palaeosol profile is compared with a much less mature profile that developed in the same rhyolite, but that was aborted earlier by the local emplacement of a lenticular lahar and a mafic flow on top of it.

Two contrasting types of palaeosols in the basal mafic succession of the Dunn Point Formation were interpreted to have been controlled by climatic cyclicity with a larger time amplitude than that separating the successive mafic flow emplacements (Jutras *et al.* 2012). In other words, each palaeosol shows evidence of having evolved under only one of the two inferred palaeoclimates, as a hybrid facies between the two types of palaeosol was not found. However, based on measured

†Author for correspondence: pierre.jutras@smu.ca

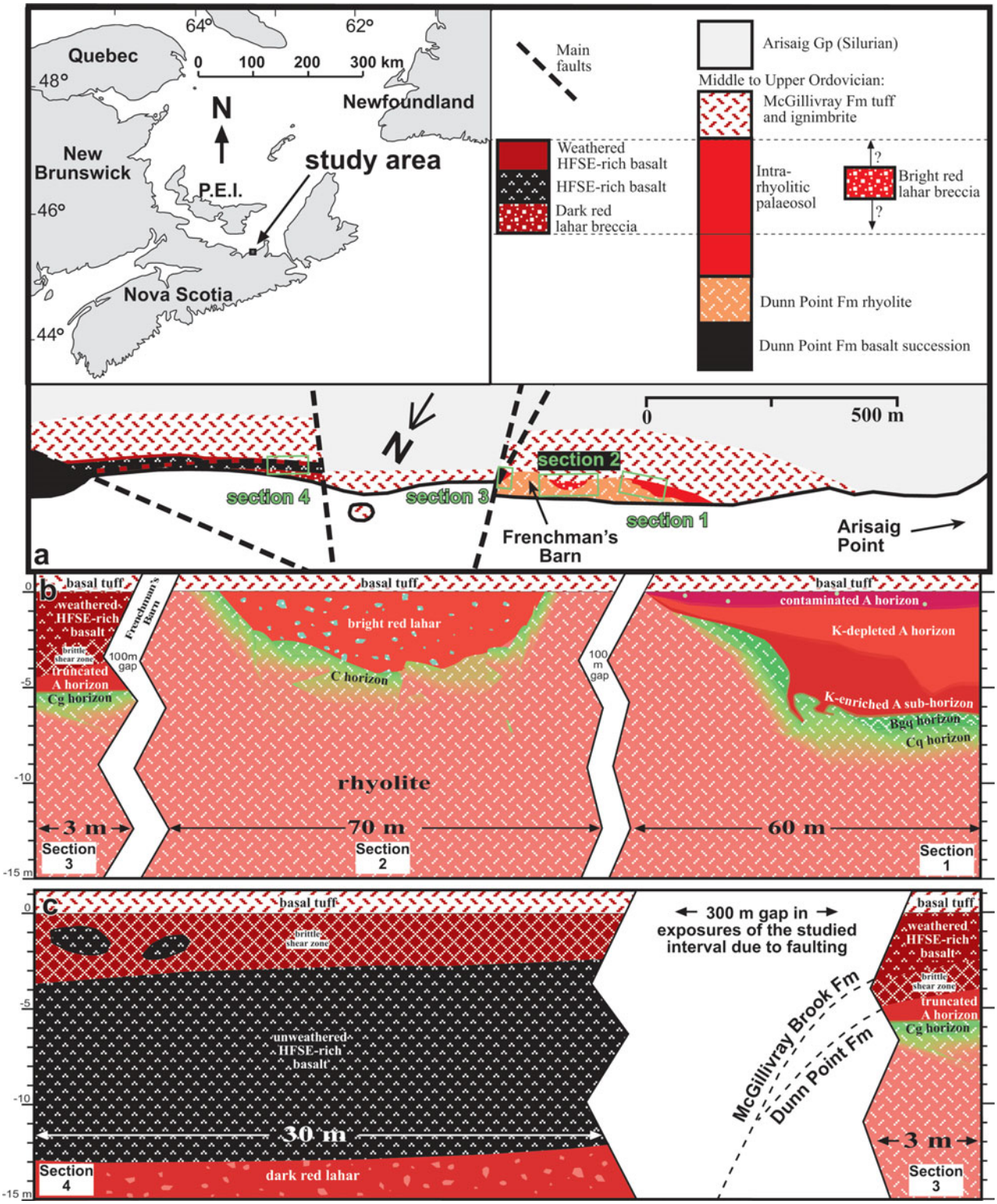

Figure 1. (Colour online) (a) Simplified geology of the study area (modified from Boucot *et al.* 1974), and section localities. The inset situates the study area within eastern Canada. (b, c) Lateral variations between unweathered rhyolite of the uppermost Dunn Point Formation and the lowermost tuff of the McGillivray Brook Formation.

thicknesses and strain calculations, the intra-rhyolitic palaeosol was up to at least 20 times thicker than any of the intra-basaltic profiles prior to burial compaction (Jutras, Quillan & LeForte, 2009), despite being hosted by rocks that are typically more resistant to weathering. The intra-rhyolitic palaeosol is therefore inferred to have evolved during a much longer time period than the underlying intra-basaltic profiles. Hence, one important purpose of this study is to see the outcome of this inferred climatic cyclicity in a weathering profile that may have developed through more than one cycle. Although information regarding palaeoclimate change has often been obtained from stacked successions of palaeosols (e.g. Kraus, 1999 and references therein;

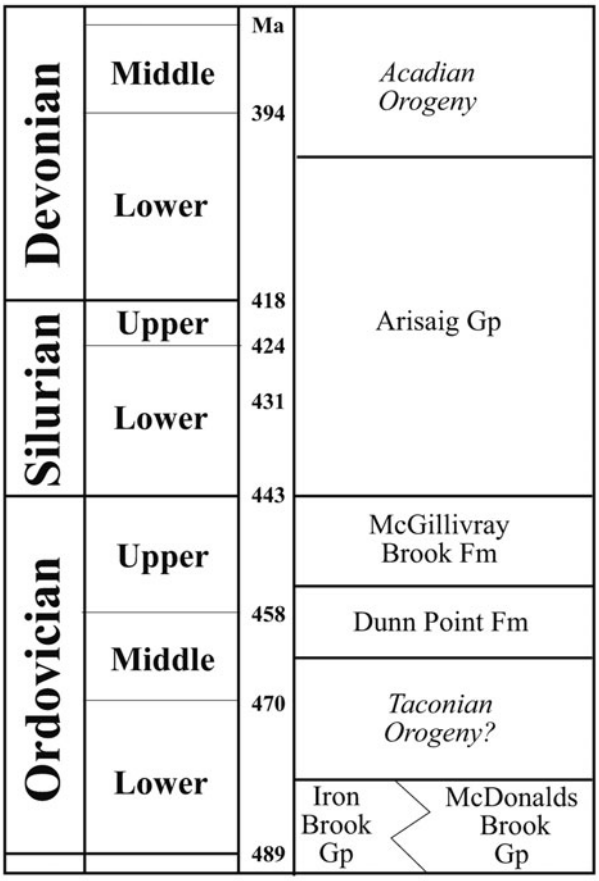

Figure 2. Stratigraphic table for the early to middle Palaeozoic of the Arisaig area in northern Nova Scotia (based on the time scale of Okulitch, 2004, and on the stratigraphic nomenclature of Boucot *et al.* 1974, Murphy, Keppie & Hynes, 1991, and Murphy, Hamilton & Leblanc, 2012).

Kleinert & Strecker, 2001; Buggle *et al.* 2009, 2013, 2014; Metzgera & Retallack, 2010; Peryam, Dorsey & Bindeman, 2011; Jutras *et al.* 2012), this is the first reported evidence of climate fluctuations within a single profile that has evolved over a very long period of time.

2. Geological and palaeoenvironmental settings

The two studied shoreline sections of the intra-rhyolitic palaeosol are separated by ~ 300 m along the Northumberland Strait near Arisaig, Nova Scotia (sections 1 and 3 on Fig. 1a). The rhyolite and its weathering profile form the upper part of the Middle to Upper Ordovician Dunn Point Formation (*sensu* Murphy, Hamilton & Leblanc, 2012), which is mainly characterized by a succession of mafic flows unconformably above metamorphic rocks of the Lower Cambrian to Lower Ordovician Iron Brook Group and laterally equivalent McDonalds Brook Group (Murphy, Keppie & Hynes, 1991) (Fig. 2). The rhyolite was dated at ~ 460 Ma (± 3.4) (Middle to Upper Ordovician) based on U–Pb isotopes in zircons by Hamilton & Murphy (2004), which places it approximately at the Middle to Late Ordovician boundary (458 ± 4 Ma according to Okulitch (2004), or ~ 461 Ma according to Walker & Geissman (2009). These rocks are part of the small palaeocontinent of Avalonia, which was at 42° S latitude at the time of basalt cooling according to the palaeomagnetic study of van der Voo & Johnson (1985). If the latter estimation is correct, the warm and humid climate signature in intra-basaltic palaeosols of the Dunn Point Formation (Jutras *et al.* 2012) would support the view that the Middle to Late Ordovician transition was still under greenhouse conditions, although at the eve of a minor, latest Ordovician ice age (Saltzman & Young, 2005). However, Jutras *et al.* (2012) pointed out some substantial discrepancies between the palaeomagnetic history of Avalonia, in relationship to that of Laurentia, and the timing of deformation episodes on both continents, casting doubt on the accuracy of palaeomagnetic data from van der Voo & Johnson (1985) and palaeocontinental reconstructions that incorporated them (e.g. Murphy, Hamilton & Leblanc, 2012).

The Dunn Point Formation is concordantly overlain by the Upper Ordovician McGillivray Formation (Fig. 2), which includes volcaniclastic rocks and a previously unreported mafic flow, and which is topped by a continuous succession of volcanogenic sedimentary rocks (tuff and ignimbrite). The top of the volcanogenic succession was dated at 454.5 ± 0.7 Ma (U–Pb) using zircons (Murphy, Hamilton & Leblanc, 2012).

According to Murphy, Dostal & Keppie (2008), the Dunn Point Formation basalts formed from a tholeiitic magma emplaced in a continental, back-arc setting. They also suggested that the overlying flow-banded rhyolite formed by partial melting of the continental crust due to high heat flow associated with the rise of basaltic magma, which would account for the temporal and spatial association between the basalts and the rhyolite. However, Murphy, Hamilton & Leblanc (2012) pointed out that similarities in Sm–Nd isotopic characteristics and in ranges of incompatible element ratios between the mafic and felsic rocks of the Dunn Point Formation suggest that the latter may be mostly a fractionation product of the former.

The intra-basaltic palaeosols of the Dunn Point Formation were originally referred to as laterites by Dewey & Ziegler (*in* Boucot *et al.* 1974), and later classified as Inceptisols and weakly developed Oxisols by Feakes, Holland & Zbinden (1989) in accordance with the United States Department of Agriculture (USDA) Soil Classification scheme at the time. However, because warm and humid environments now favour the development of a lush vegetation cover, modern, unfarmed Oxisols of such environments are characterized by low pH soil water, which typically ranges between 4 and 5.5 (e.g. Ismail, Shamshuddin & Syed Omar, 1993; Oliveira *et al.* 2000; Chapuis-Lardy, Brossard & Quiquampoix, 2001; Anda *et al.* 2008; Schaefer, Fabris & Ker, 2008; Shamshuddin & Anda, 2012). In contrast, the intra-basaltic Ordovician palaeosols of the Dunn Point Formation show evidence of having evolved in warm, humid and alkaline conditions, which cannot be

achieved in today's vegetated world, and which resulted in soil characteristics that have no modern equivalents (Jutras, Quillan & LeForte, 2009; Jutras *et al*. 2012). The Dunn Point Formation experienced deep burial under the thick Silurian marine sedimentary rocks and Lower Devonian continental clastic rocks of the Arisaig Group (Figs 1, 2) and subsequent folding during the Middle Devonian Acadian Orogeny, but it is not significantly metamorphosed (Hamilton & Murphy, 2004).

3. Field relationships

The thick rhyolite at the top of the Dunn Point Formation is well exposed at Frenchman's Barn, a ~ 120 m wide differential erosion knob of rhyolite that dominates the coastal landscape in the study area (Figs 1, 3a). A tight network of vertical quartz veinlets permeates the rhyolite at Frenchman's Barn and is interpreted to have made this unit locally more resistant to erosion in that area.

The rhyolite at Frenchman's Barn is sharply overlain by the lowermost tuff of the McGillivray Brook Formation (Figs 1, 3a). However, immediately to the southwest of the knob, an up to 4.5 m thick lahar breccia lens separates the two units (Figs 1, 3a). This lahar breccia is no more than 70 m wide, pinching out to the southwest into another area where the lowermost tuff directly overlies the rhyolite (Fig. 1b). Another ~ 100 m to the southwest, a pinching-in palaeosol separates fresh rhyolite from the lowermost tuff, evolving gradually to a thickness of ~ 8.5 m (measured and sampled Section 1) over a distance of ~ 60 m (Figs 1, 3b).

On the NE flank of Frenchman's Barn, the upper part of the rhyolite transitions into an incomplete ~ 1.5 to ~ 2.5 m thick palaeosol that is truncated by a ~ 0.5 to ~ 1.5 m thick brittle shear zone, which separates it from a ~ 2 to ~ 3 m thick lens of weathered mafic rocks that lie concordantly below the lowermost tuff (Figs 1b, 3c). This little remnant of weathered mafic rocks is part of a lenticular succession of lahar and basalt that occurs between the rhyolite and the lowermost tuff to the northeast of Frenchman's Barn (Fig. 1c), marking the base of the McGillivray Brook Formation in that area. The McGillivray Brook Formation basalt that overlies the rhyolite is characterized by very high contents of high-field-strength elements (HFSEs; e.g. 455 ppm of Zr in sample S4-2; Table 2) compared to the Dunn Point Formation basalts that underlie the rhyolite (e.g. 131 to 194 ppm of Zr according to Jutras *et al.* 2012). Based on sections 9 and 10 of Boucot *et al.* (1974), the post-rhyolitic mafic flow (McGillivray Brook Formation) was mistakenly assigned to the mafic succession below the rhyolite (Dunn Point Formation) by these workers and subsequent workers (e.g. Murphy, Hamilton & Leblanc, 2012).

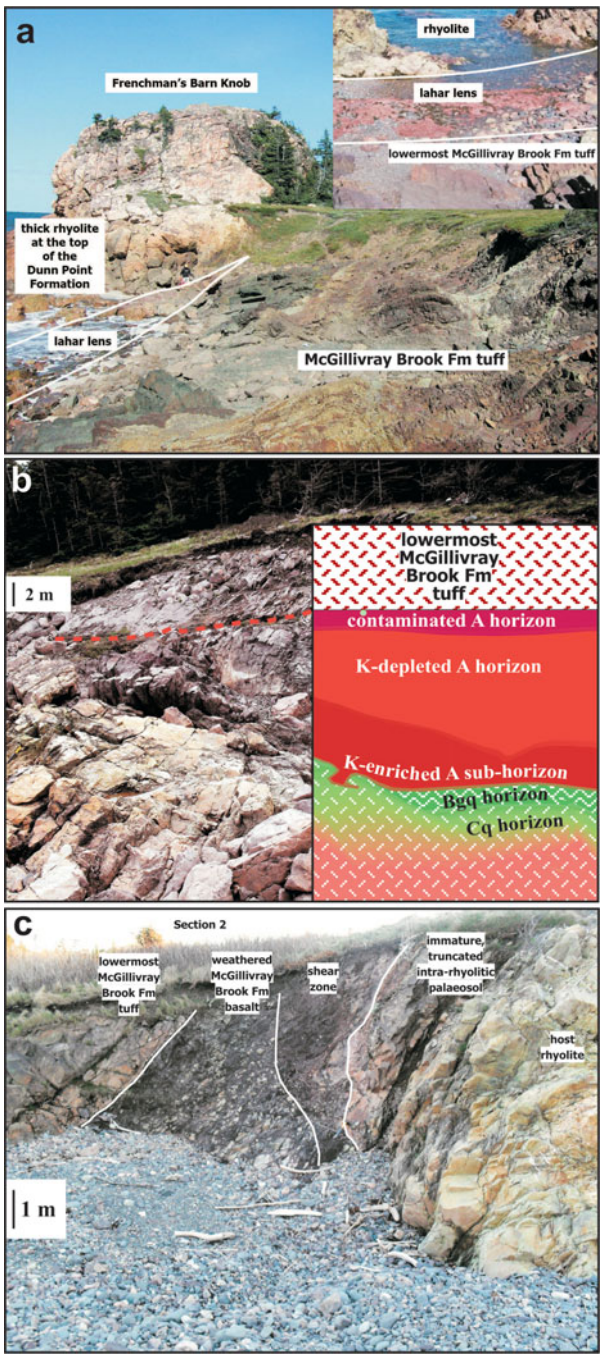

Figure 3. (Colour online) (a) Rhyolite knob (Frenchman's Barn) and overlying lahar breccia lens and tuff (Section 2). (b) Mature intra-rhyolitic palaeosol profile at Section 1. (c) Immature intra-rhyolitic palaeosol profile at Section 3 truncated by a shear zone that separates it from an overlying HFSE-rich, weathered basalt lens.

4. Petrography of the intra-rhyolitic weathering profile and overlying units

4.a. Analytical methods

Mineral and geochemical contents of 33 samples of the intra-rhyolitic weathering profile and directly overlying rocks were determined by thin-section petrography and X-ray diffraction (XRD) analyses (Siemens D5000 diffractometer hosted at the Université du Québec à Montréal; results in Table 1), and by X-ray fluorescence

Table 1. Semi-quantitative X-ray diffraction (XRD) analyses performed at the Département des Sciences de la Terre et de l'Atmosphère de l'Université du Québec à Montréal, Canada

	Sample	Depth cm	Amorphous vol. %	Quartz vol. %	Pyrophyllite vol. %	Chlorite vol. %	Biotite vol. %	Muscovite vol. %	Albite vol. %	K-feldspars vol. %	Haematite vol. %
	S4-3 (shear zone)	−300	5	42		6		19	15		13
Section 4	**S4-2 (McG. Br. basalt)**	−1000		31	[+1 % calcite]	19	1		40		8
	S4-1 (dark red lahar)	−1600		66	3	4*		5	14	1	7
	S3-9 (basal tuff)	0		90				6			4
	S3-8 (weathered basalt)	−100		32	3			28	9		28
	S3-7 (weathered basalt)	−200		45	2			26	6		21
	S3-6 (shear zone)	−250	3	66		4		5	14	1	7
Section 3	**S3-5 (shear zone)**	−340		46		2		37	4	1	10
	S3-4 (shear zone)	−400		49		1		37	5	1	7
	S3-3 (reddish-brown A)	−490	5	80			2	10	1		2
	S3-2 (green Co)	−560	5	60				9	13	12	1
	S3-1 (rhyolite)	−600		69	[+1 % pyroxene]		1	21	8		
Section 2	**S2-1 (bright red lahar)**	−90		35				54	2		9
	S1-20 (basal tuff)	+55		75	3			14			8
	S1-19 (basal tuff)	0	3	70	2			18			7
	S1-18 (contaminated A)	−5	10	6	2	2*		70	1	1	8
	S1-17 (contaminated A)	−80	2	9	3	26*		51			9
	S1-16 (massive red A)	−140		7	4	30*		49			10
	S1-15 (massive red A)	−190	5	6	16	30*		31			12
	S1-14 (massive red A)	−260	4	15	35	16*		21			9
	S1-13 (massive red A)	−325	5	17	31	22*		15			10
	S1-12 (massive red A)	−375	4	5	26	42*		13			10
	S1-11 (massive red A)	−410	1	13	29	2*		38			17
Section 1	**S1-10 (massive red A)**	−480	1	8	31	1*		45			14
	S1-9 (reddish AB)	−550	4	51	1	1*		36			7
	S1-8 (reddish AB)	−600		56	2			35			7
	S1-7 (green Bgq)	−625		90			4	5			1
	S1-6 (green Bgq)	−650	2	87			5	6			
	S1-5 (green Bgq)	−675	8	77			5	7	1	2	
	S1-4 (green Bgq)	−700	5	75			2	3	8	7	
	S1-3 (pink Cq)	−750	6	63			1	3	14	13	
	S1-2 (pink Cq)	−825	4	78			3	7	4	3	1
	S1-1 (rhyolitic host rock)	−900		19			2	4	66	8	1

(*) – chamosite; McG. Br. – McGillivray Brook Formation. Depths are in centimetres below the lowermost tuff of the McGillivray Brook Formation.

(XRF) analyses (Phillips PW2400 X-ray spectrometer hosted at the Regional Geochemical Centre of Saint Mary's University; results in Table 2). Three samples were selected to compare the host rhyolite (sample S1-1) to the B (sample S1-4) and A (sample S1-16) horizon material of the intra-rhyolitic palaeosol on a Leo 1450 VL scanning-electron microscope (SEM) hosted at Saint Mary's University (Halifax, Nova Scotia) and operating at an accelerating voltage of 20 kV and a beam current ranging from 5 to 20 nA. Secondary X-ray mapping of elements with concentrations above the XRF detection limit of 0.1 wt. % was done with energy dispersive spectroscopy (EDS) on carbon-coated polished thin-sections of these three samples (Figs 4, 5, 6).

To estimate element mobility in the weathering profiles, we calculated the element-mass-transfer coefficient of Anderson, Dietrich & Brimhall (2002; modified from Brimhall *et al.* 1992) for selected elements, assuming Zr-immobility (Fig. 7a, b, c). Zirconium was selected as the reference immobile element because it is considered to be least mobile in weathering environments based on lab experiments (Hodson, 2002), and also because it shows a regular covariance with the almost equally resistant Nb (Table 2), suggesting that both elements were relatively immobile in our profiles. In contrast, Y shows much variance with both Zr and Nb (Table 2), suggesting a substantial mobility of this element in our profiles during weathering. Although Y is usually immobile in hydrothermal alteration processes, which has led to its widespread use in geochemical discrimination diagrams (e.g. Winchester & Floyd, 1977), it has been demonstrated to be quite mobile in soils of warm and humid environments (Hill, Worden & Meighan, 2000).

Variations of Y contents in relation to Zr contents in the intra-rhyolitic palaeosol are plotted on Figure 7a, b, c along with all major elements with concentrations that exceed the XRF detection limit of 0.1 % in the host rock. The suffix symbols used for the palaeosol horizons are based on the USDA Keys to Soil Taxonomy (Soil Survey Staff, 2010). Because there is no suffix for K-enrichment in soils, as this element does not typically illuviate in modern soil horizons, we refer to this important characteristic of some of the herein studied palaeosol horizons in full (i.e. as 'K-enriched'; Fig. 7a, b, c).

4.b. The unweathered rhyolite host rock

The rhyolite host rock at Section 1 shows an albite-dominated composition (66 %; Table 1) and therefore high Na and low Ca contents (Table 2), which suggests that it was significantly albitized during and shortly after emplacement. It is composed of 19 % quartz, 8 % K-feldspars, 4 % muscovite, 2 % biotite and 1 % haematite (Table 1; Figs 4, 8). Traces of anatase and ilmenite are also observable on the element maps as small areas of high Ti concentrations (Fig. 4).

At Section 3, the rhyolite host rock is part of the silica-enriched zone of Frenchman's Barn, which resulted in a host rock with only 29 % feldspars, compared with 73 % at Section 1, and 69 % quartz, compared with 19 % at Section 1 (Table 1). Chemically, it resulted in a host rock at Section 3 that is ~ 10 % richer in SiO_2 and ~ 30 % poorer in Al_2O_3 than at Section 1 (Table 2).

4.c. Thick and mature intra-rhyolitic weathering profile at Section 1

Among available exposures, the intra-rhyolitic palaeosol profile is thickest and best developed at the level of Section 1, where it reaches ~ 8.5 m in thickness (Fig. 1). The base of the weathering profile is very irregular and pinches out less than 60 m to the northeast (Fig. 1b). Field evidence, such as the gradational nature of vertical changes in colour and texture, suggests that the weathering profile below the tuff at Section 1 is entirely hosted by rhyolite. This conclusion is also supported by relatively stable Zr/TiO_2 and Zr/Nb ratios, which, respectively, range from 3.9 to 4.9 and 6.5 to 8.8 in the intra-rhyolitic profile (Table 2). In the overlying tuff, Zr/TiO_2 ratios drop to 2.6 and 2.9, and Zr/Nb ratios increase to 11.4 and 12.0 (Table 2).

4.c.1. Slightly weathered rhyolite (K-enriched Cq horizon) at the base of the profile

The weathering profile at Section 1 starts with a ~ 1.5 m thick region of slightly weathered rhyolite (C horizon) that fully preserved its volcanic textures, but that is strongly enriched in quartz (63–78 %, from 19 %) and strongly depleted in feldspars (7–27 %, from 73 %; Fig. 8). This slightly weathered rhyolite shows pronounced Na and Mg depletion, relatively stable Al, irregular concentrations of Fe, moderate enrichment in Ti, and pronounced enrichment in K, Y and Si (Fig. 7a, b). It is therefore categorized as a K-enriched Cq horizon.

4.c.2. Green, K-enriched Bgq horizon

The Cq horizon grades upwards into a ~ 1 m thick mottled, green, K-enriched Bgq horizon (i.e. enriched in reduced Fe and silica). This horizon is even more enriched in quartz (85–89 %, from 63–78 % in the Cq horizon), and even more strongly depleted in feldspars (3–7 % in the lower part of the horizon to < 1 % in the upper part, from 7–27 % in the Cq horizon) (Table 1; Fig. 8), which are mainly found in small areas that preserved the texture and composition of the parent rhyolite. The bulk of the Bgq horizon is composed of globular accumulations of cryptocrystalline quartz mingling with tightly interstratified muscovite (3–7 %; Table 1) and biotite (2–5 %; Table 1) in which Al, K, Fe and Mg are evenly scattered (Fig. 5). In contrast, Ti is discretely concentrated in sparsely disseminated ilmenite (where paired with high Fe concentrations) and anatase crystals that float in the micaceous matrix (Fig. 5). This

Table 2. X-ray fluorescence analyses

	Sample	Depth Cm	SiO_2 wt %	TiO_2 wt %	Al_2O_3 wt %	Fe_2O_3 wt%	MnO wt %	MgO wt %	CaO wt %	Na_2O wt %	K_2O wt %	P_2O_5 wt %	LOI wt %	Nb ppm	Y ppm	Zr ppm
	S4-3 (shear zone)	−300	38.15	3.302	22.21	22.57	0.05	0.84	0.49	0.37	6.33	0.27	5.79	44	49	624
Section 4	**S4-2 (McG. Br. basalt)**	−1000	51.36	2.40	15.61	12.81	0.30	3.99	4.49	3.95	0.60	0.55	4.41	30	43	455
	S4-1 (dark red lahar)	−1600	66.47	0.80	13.41	8.71	0.07	0.77	1.61	1.99	2.94	0.18	3.46	69	81	738
	S3-9 (basal tuff)	0	76.52	0.26	12.78	2.82	0.02	0.29	0.04	0.13	4.07	0.06	2.94	106	241	1971
	S3-8 (weathered basalt)	−5	42.45	3.03	22.07	17.38	0.04	0.43	1.17	0.18	7.17	0.91	5.28	88	135	889
	S3-7 (weathered basalt)	−120	46.14	2.87	21.32	14.61	0.04	0.43	1.29	0.13	6.98	1.01	5.54	74	112	823
	S3-6 (shear zone)	−250	53.45	0.75	25.33	8.12	0.02	0.27	0.17	0.08	7.65	0.18	4.20	92	84	714
Section 3	**S3-5 (shear zone)**	−340	54.38	0.75	24.81	7.43	0.02	0.27	0.06	0.17	7.60	0.10	4.27	79	55	687
	S3-4 (shear zone)	−400	54.86	0.75	26.10	5.61	0.03	0.15	0.03	0.17	7.90	0.09	4.27	110	104	926
	S3-4 (reddish-brown A)	−490	72.68	0.25	16.63	1.78	0.01	0.16	0.03	0.13	4.92	0.03	3.33	73	61	613
	S3-3 (reddish-brown A)	−520	68.83	0.28	18.40	2.20	0.02	0.32	0.03	0.84	6.14	0.03	2.84	83	83	718
	S3-2 (green Co)	−560	72.12	0.24	15.93	0.98	0.01	0.19	0.04	1.64	6.83	0.03	1.60	76	89	525
	S3-1 (rhyolite)	−600	81.15	0.15	10.64	0.30	0.00	0.06	0.06	3.72	3.10	0.03	0.61	43	87	357
Section 2	**S2-1 (bright red lahar)**	−90	51.60	0.43	29.36	6.24	0.01	0.06	0.01	0.17	7.40	0.04	4.48	121	54	1098
	S1-20 (basal tuff)	+55	65.53	0.66	16.56	7.08	0.04	0.34	0.05	0.14	5.21	0.05	3.81	189	269	2264
	S1-19 (basal tuff)	0	57.05	0.84	22.46	4.90	0.02	0.37	0.10	0.13	6.47	0.11	6.93	283	329	3221
	S1-18 (contaminated A)	−5	44.89	0.54	34.08	4.75	0.01	0.16	0.04	0.15	9.82	0.07	5.37	168	61	1398
	S1-17 (massive red A)	−80	43.14	0.67	35.05	5.81	0.01	0.09	0.02	0.15	9.38	0.06	5.40	201	19	1651
	S1-16 (massive red A)	−140	42.68	0.77	35.39	7.46	0.01	0.12	0.04	0.06	5.19	0.11	8.27	251	53	1806
	S1-15 (massive red A)	−190	42.77	0.56	35.49	7.41	0.00	0.11	0.03	0.05	4.00	0.04	9.95	184	37	1355
	S1-14 (massive red A)	−260	45.01	0.47	37.73	5.00	0.00	0.06	0.02	0.03	3.38	0.13	8.38	144	46	1188
	S1-13 (massive red A)	−325	43.37	0.57	36.21	7.47	0.00	0.07	0.02	0.03	4.09	0.04	8.28	160	73	1162
Section 1	**S1-12 (massive red A)**	−375	45.08	0.49	35.07	7.24	0.03	0.06	0.02	0.03	2.26	0.04	10.05	153	65	1159
	S1-11 (massive red A)	−410	42.15	0.51	34.50	8.31	0.05	0.06	0.01	0.13	6.67	0.02	7.26	150	56	1310
	S1-10 (massive red A)	−480	43.75	0.49	33.88	8.00	0.01	0.09	0.03	0.14	6.86	0.04	6.54	142	82	1252
	S1-9 (reddish AB)	−550	56.29	0.39	26.40	4.39	0.00	0.10	0.03	0.14	7.54	0.11	4.22	114	298	955
	S1-8 (reddish AB)	−600	52.57	0.40	27.80	5.71	0.01	0.15	0.04	0.16	7.89	0.10	4.76	116	270	999
	S1-7 (green Bgq)	−625	80.83	0.17	11.35	1.49	0.01	0.19	0.02	0.10	3.49	0.03	2.13	49	107	403
	S1-6 (green Bgq)	−650	81.53	0.17	11.27	1.07	0.02	0.16	0.02	0.09	3.55	0.03	1.94	48	124	395
	S1-5 (green Bgq)	−675	78.80	0.19	13.42	1.19	0.01	0.15	0.02	0.06	4.31	0.04	2.31	63	108	407
	S1-4 (green Bgq)	−700	81.15	0.17	11.67	1.30	0.02	0.13	0.03	0.07	3.73	0.03	2.19	49	60	349
	S1-3 (pink Cq)	−750	81.33	0.17	10.96	0.82	0.00	0.04	0.05	2.84	2.60	0.03	1.18	52	78	361
	S1-2 (pink Cq)	−825	82.73	0.15	9.81	0.46	0.00	0.02	0.04	1.40	3.81	0.03	1.10	47	73	316
	S1-1 (rhyolitic host rock)	−900	73.67	0.20	15.32	1.01	0.01	0.11	0.07	5.62	2.90	0.03	1.05	60	72	495

Detection limit is 0.1 % for major elements (fusion method), and 1 ppm for minor elements (pressed pellets method). McG. Br. – McGillivray Brook Formation. Depths are in centimetres below the lowermost tuff of the McGillivray Brook Formation.

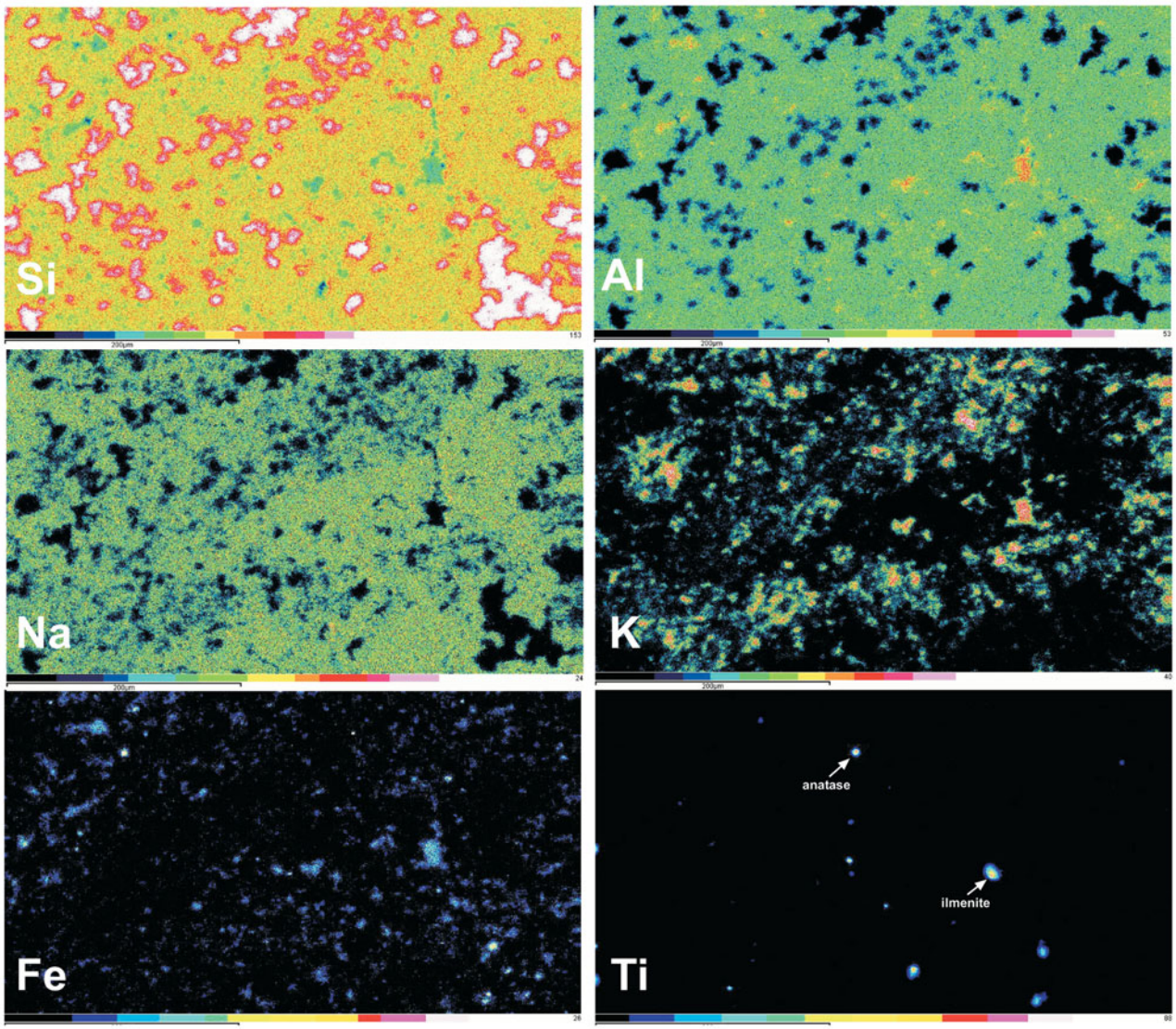

Figure 4. (Colour online) SEM-EDS maps showing the distribution of Si, Al, Na, K, Fe and Ti in the rhyolitic host rock (sample S1-1) at Section 1, which is dominated by albite (green areas on the Na map) and quartz (white areas on the Si map). Potassium is distributed in muscovite, biotite and K-feldspars. Iron is in biotite, haematite and traces of ilmenite and pyroxene. Titanium is in traces of anatase and ilmenite.

horizon is strongly depleted in Na, slightly enriched in Al and Ti, and strongly enriched in Si, K, Y, Fe and Mg (Fig. 7a, b).

4.c.3. Brownish-red, K-enriched A sub-horizon

The green Bgq horizon transitions upwards into a ~ 1 m thick brownish-red, mottled horizon that is much more micaceous (35–36 % from 5–12 % in the Bgq horizon, and featuring no more biotite) and haematitic (7 %, from 0–1 % in the Bgq horizon, at the expense of biotite), and less quartzitic (51–56 %, from 75–90 % in the Bgq horizon) than in the underlying horizon (Table 1; Fig. 8). The haematite forms distinct, sinuous bands of opaque material separated by the micaceous matrix. This horizon shows pronounced Na, Mg and Si-depletion, slight Al-depletion, Ti-immobility, pronounced K-enrichment, and very pronounced Y and Fe-enrichment (Fig. 7a, b). As will be subsequently discussed, the accumulation of Fe in this horizon is not interpreted as pedogenic and is therefore not included as a soil horizon suffix.

4.c.4. Bright red A sub-horizon

The next ~ 4.5 m is a massive to slaty, bright red A sub-horizon, which includes areas with white spots of muscovite that tend to elongate parallel to the poorly defined, parallel-to-bedding schistosity. As muscovite is ubiquitous in the material of the A horizon, these white spots are more precisely areas from which Fe was leached (Fig. 6). Interestingly, Ti is found exclusively in anatase within these white spots, whereas it is mainly found in ilmenite (i.e. combined with Fe) within the red bulk of the bright red A sub-horizon material (Fig. 6). Away from these Fe-free areas, the bulk of this sub-horizon is characterized by closely interstratified pyrophyllite (4–35 %), muscovite (13–49 %) and

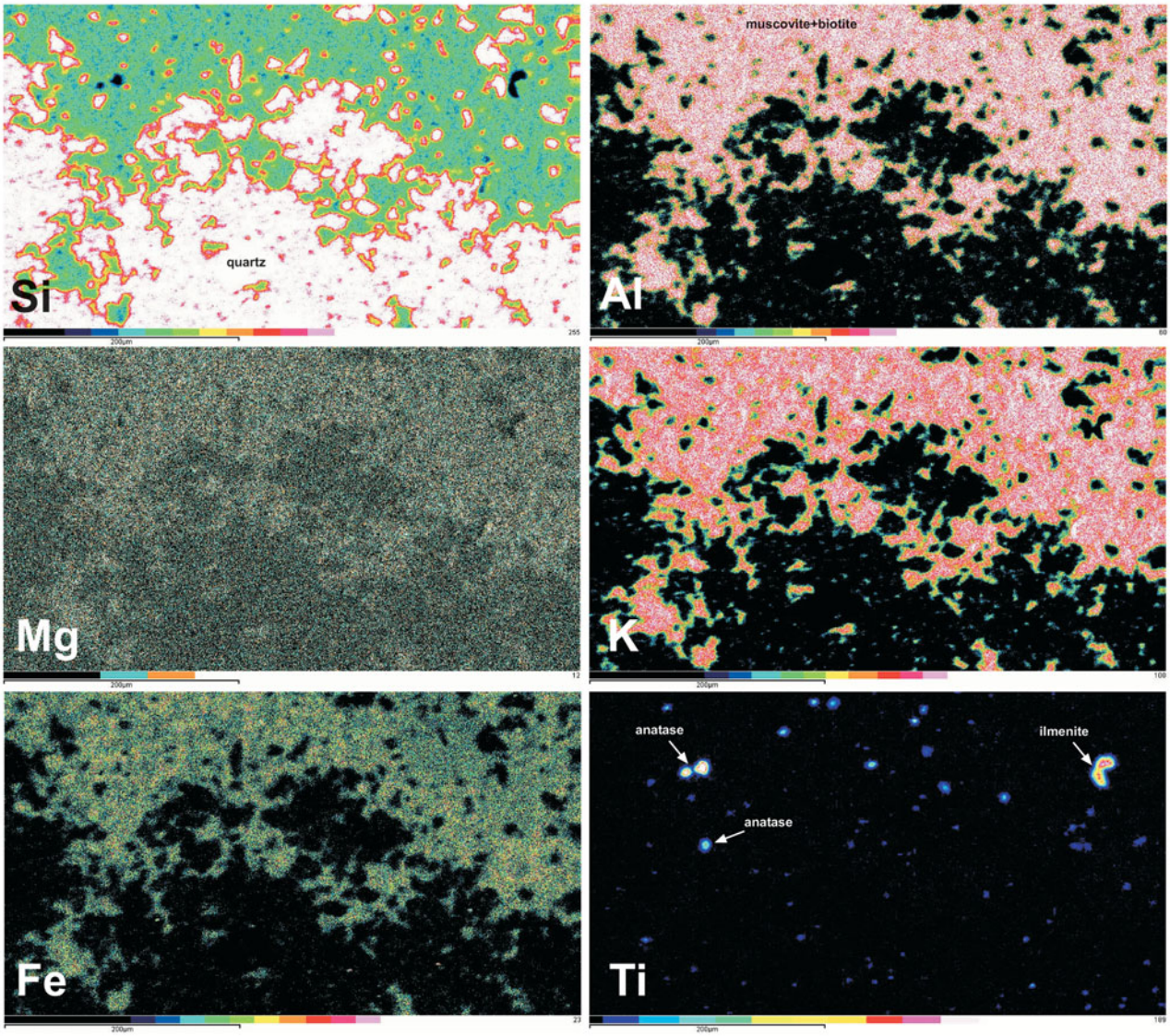

Figure 5. (Colour online) SEM-EDS maps showing the distribution of Si, Al, Mg, K, Fe and Ti in the green Bgq horizon (sample S1-4) at Section 1, which is dominated by quartz (white areas on the Si map) and tightly interstratified muscovite and biotite (areas of high Al, Mg, K and Fe concentrations). Potassium is distributed in muscovite, biotite and K-feldspars. Iron is in biotite, haematite and traces of ilmenite and pyroxene. Titanium is in traces of anatase and ilmenite, but also disseminated in small concentrations within the micaceous matrix.

chamosite (1–42 %), with finely disseminated cryptocrystalline quartz (5–17 %), specks of haematite (9–17 %) and specks of gibbsite that are well observable as areas of high Al and no Si on the element maps, and that seemingly form the bulk of the 0–5 % amorphous fraction on XRD (Table 1; Figs 6, 8). The haematite is Ti-rich and is surrounded by high concentrations of K, which are also found at the rim of large chamosite crystals (Fig. 6), suggesting that K was already in place when Fe-enrichment occurred.

This sub-horizon shows strongly depleted Na, Y, Mg and Si, strongly to slightly depleted K, stable to moderately depleted Al, stable Ti, and strongly enriched Fe (Fig. 7a, b). Again, because the Fe-enrichment is not interpreted as pedogenic (see Section 6), it is not included as a soil horizon suffix.

One important pattern in the plot of vertical mass gains and losses for this sub-horizon is that of Al, which is stable in the middle of the sub-horizon, but which shows significant depletion in its lower and upper parts (Fig. 7b). This peculiar behaviour of Al in the profile will be discussed at length in a subsequent section.

4.c.5. Purplish-red and contaminated A sub-horizon

The massive, bright red A sub-horizon grades upwards into ~ 1 m of a purplish-red material that is sharply overlain by tuff. Although crumbly on outcrop due to modern weathering, this uppermost part of the A horizon is aphanitic and massive in thin-section. Contamination related to tuff emplacement is apparent, especially in the uppermost sample, which shows significant increases in Y, Mg and K contents with regards to Zr (Fig. 7a). This contaminated section is also less enriched in Fe than the rest of the A horizon (Fig. 7b).

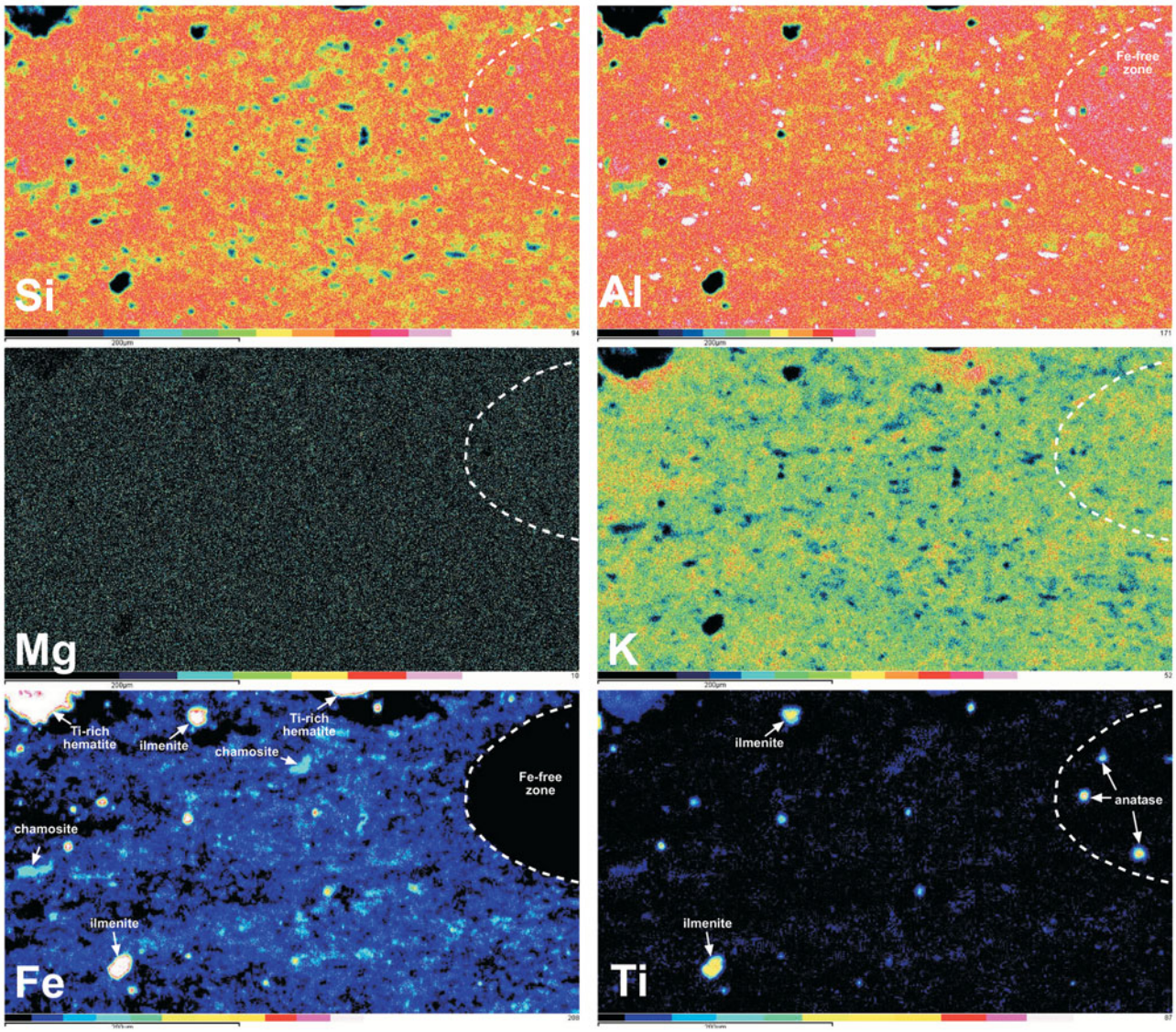

Figure 6. (Colour online) SEM-EDS maps showing the distribution of Si, Al, Mg, K, Fe and Ti in the bright red A horizon (sample S1-16) at Section 1, which is dominated by muscovite (green and orange areas on the K map), pyrophyllite (pink areas on the Si map, closely mingling with muscovite), chamosite (green areas on the Al map and light blue areas on the Fe map), gibbsite (white specks on the Al map), disseminated haematite (in the dark blue areas of the Fe map) and concentrated Ti-rich haematite specks (white areas on the Fe map with corresponding light blue areas on the Ti map). Titanium is concentrated in anatase and ilmenite, but also in haematite specks, and it is disseminated with haematite in the matrix of phyllosilicates. Haematite specks are tightly associated with small areas of Fe-leaching, but larger Fe-free areas, such as the one delineated here, are not associated with areas of concentrated haematite and seem to represent net losses of Fe from the profile.

Detrital quartz and feldspar silts are disseminated in the uppermost sample (Table 1; Fig. 8), indicating minor sedimentary contamination at the very top of the profile. However, the marked increase in muscovite (70 %, compared with 13–49 % in the rest of the A horizon) at the expense of pyrophyllite and chamosite (2 % each, compared with, respectively, 4–35 % and 1–42 % in the underlying sub-horizon; Table 1; Fig. 8) is interpreted as authigenic and related to heat inputs at the time of tuff emplacement.

4.d. Immature, truncated weathering profile at Section 3

On the NE flank of the Frenchman's Barn knob, the weathered rhyolite is truncated by a brittle shear zone that incorporated and mixed material from the top of its weathering profile with that from an overlying weathered basalt, which is herein reported for the first time (Section 3 on Figs 1, 3c, 7d, e). Zr/TiO_2 ratios range from 3.9 to 4.6 in the intra-rhyolitic profile and jump to 34.1 and 34.9 in the overlying weathered basalt, whereas Zr/Nb ratios range from 7.8 to 8.7 in the former and 10.1 to 11.2 in the latter.

4.d.1. Green, K-enriched Cg horizon

The silicified, but unweathered rhyolite host at Section 3 transitions upwards into ~ 0.5 m of a massive, green Cg horizon that preserved some of the textures of the host rhyolite, but that only includes ~ 86 % of its

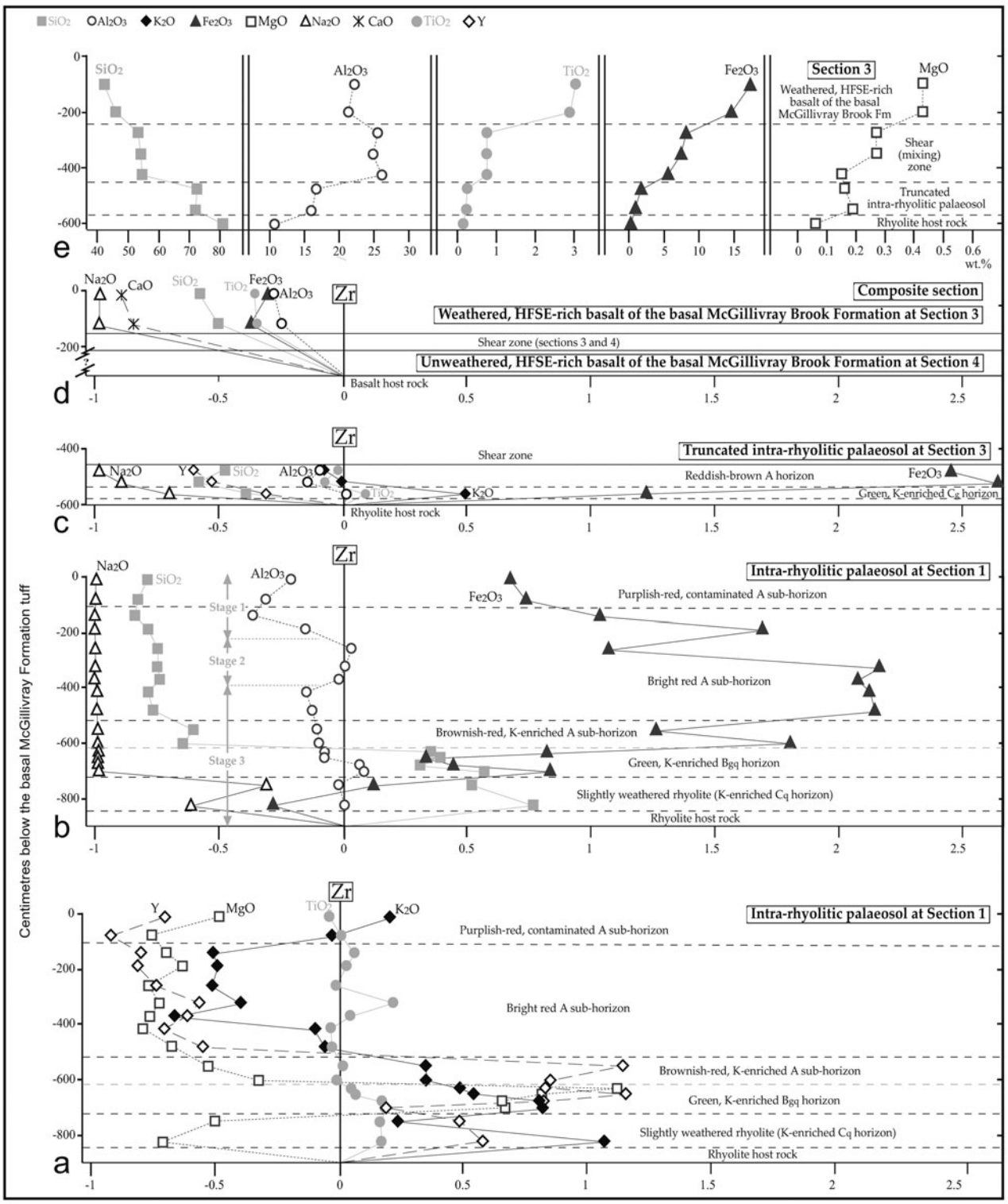

Figure 7. (a–d) Vertical mass gains and losses based on the dimensionless element-mass-transfer coefficients of Anderson, Dietrich & Brimhall (2002; modified from Brimhall *et al.* 1992) in relation to Zr: in the intra-rhyolitic palaeosol at Section 1 (a, b) and Section 3 (c) with respect to their rhyolitic host rock, and (d) in the composite intra-basaltic profile at sections 3 and 4. (e) Major element oxide concentrations in the host rhyolite and associated palaeosol at Section 3, the overlying weathered basalt lens and the shear zone material that separates the two.

original feldspar contents, and that marks a 900 % increase (from 1 to 9 %) in muscovite as a recrystallized weathering product of the feldspars (Table 1). This horizon is strongly depleted in Na, Y and Si, negligibly enriched in Al, slightly enriched in Ti, strongly enriched in K, and very strongly enriched in Fe (Fig. 7c).

4.d.2. Reddish-brown A horizon

The Cg horizon transitions upwards into a fairly well-developed reddish-brown A horizon that only includes ~ 7 % of the original feldspar content of the host rock, which translates as ~ 33 % more quartz and ~ 33 %

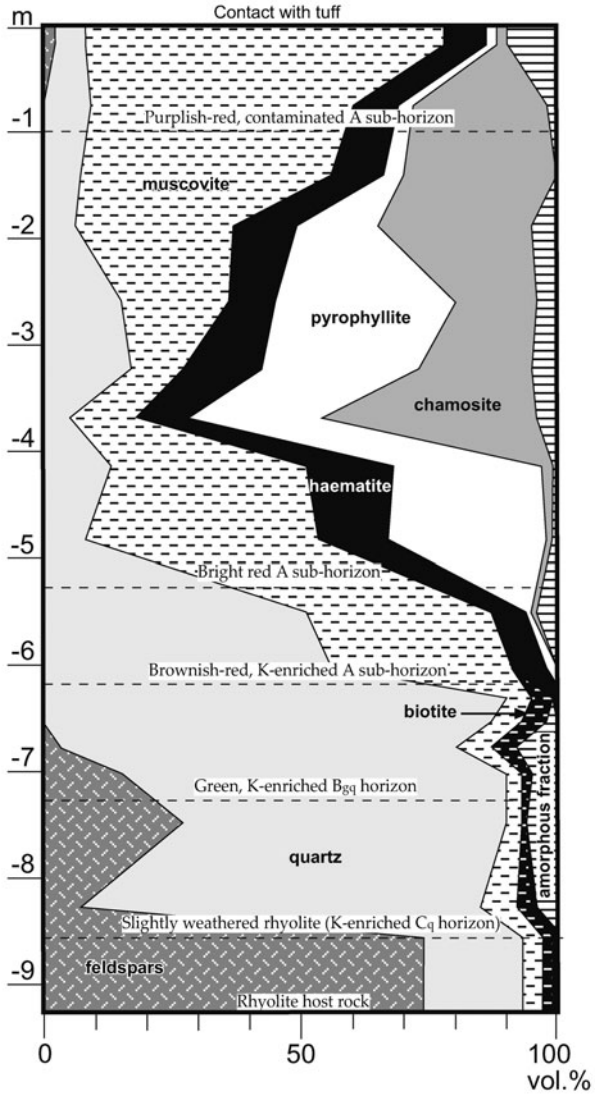

Figure 8. Mineral distribution in the intra-rhyolitic profile at Section 1 based on X-ray diffraction data from Table 1.

more muscovite than in the Cg horizon (Table 1). This horizon is very strongly depleted in Na, strongly depleted in Y and Si, slightly to negligibly depleted in Al, Ti and K, and twice as enriched in Fe than the Cg horizon (Fig. 7c), although this enrichment is once again not regarded as pedogenic (see Section 6). The top of the A horizon is missing as it was incorporated in the shear zone that separates it from the overlying weathered basalt (Fig. 7e).

4.e. Lahar breccia and weathered HFSE-rich basalt of the McGillivray Brook Formation at sections 3 and 4.

There is uncertainty regarding the original stratigraphy at Section 3 prior to the displacement of part of the succession along a brittle shear zone, which post-dates the ductile-brittle Acadian folding (Figs 1b, 3c). This displacement lowered the basal tuff and the top of an underlying mafic flow by no more than 10 m based on mapping extrapolations from the other side of Frenchman's Barn. No fresh basalt remains at Section 3, but there is possibly up to 10 m of this unit missing due to truncation by this fault.

The reddish-brown weathered basalt at the top of Section 3 is part of a volcaniclastic and mafic succession that locally marks the base of the McGillivray Brook Formation and that separates rhyolite of the underlying Dunn Point Formation from the lowermost tuff of the former unit (Fig. 1). This succession thickens substantially to the northeast, where at least 10 m of a dark red lahar deposit (base not exposed) and at least 13 m of HFSE-rich basalt (weathered top incorporated in fault breccia along with some unweathered basalt) occur below the lowermost tuff of the McGillivray Brook Formation (Section 4 on Fig. 1c).

This dark red lahar breccia includes angular pebbles of weathered rhyolite and its gritty matrix is composed of 66 % quartz, 14 % albite, 7 % haematite, 5 % muscovite, 4 % chamosite, 3 % pyrophyllite and 1 % K-feldspars (sample S4-1 in Table 1). The absence of mafic clasts and its low Ti content (0.8 wt %; Table 2) suggest that this lahar only reworked the weathering mantle of the rhyolite. Its relatively high feldspar content does not suggest any substantial weathering period separating it from the overlying basalt.

As the intra-basaltic weathering profile is truncated by shearing at its base at Section 3 and at its top at Section 4, a proper assessment of vertical mass gains and losses cannot be done for this profile, but some clues can nonetheless be derived from a reconstruction between the two sections Fig. 7d). Assuming Zr-immobility, the exposed upper part of the weathering profile shows moderate depletion in Al, Fe and Ti, strong depletion in Si, and a nearly complete eradication of Mg, Ca and Na (Fig. 7d). Similar to the intra-basaltic profiles that occur below the rhyolite, in the Dunn Point Formation, it shows over 500 % enrichment in K relative to Zr (not plotted on Fig. 7d), which cannot be explained by pedogenic processes, and which Jutras *et al.* (2012) associated with a shallow burial eodiagenetic enrichment issued from the K-rich rhyolite. The unweathered but albitized and chloritized basalt at Section 4 evolves from 40 % albite, 31 % quartz, 19 % mixed chlorites, 8 % haematite and 1 % biotite (sample S4-2 in Table 1) to 32–45 % quartz, 26–28 % muscovite, 21–28 % haematite, 6–9 % albite and 2–3 % pyrophillite (samples S3-7 and S3-8 in Table 1).

4.f. Lahar breccia lens at Section 2

A well-exposed lens of bright red, angular lahar deposit separates the rhyolite from the lowermost tuff of the McGillivray Brook Formation on the west side of Frenchman's Barn, at Section 2 (Figs 1, 3a). The lahar breccia lens is ~ 70 m wide and ~ 4.5 m thick in its thickest portion. It includes angular pebbles and cobbles of rhyolite and red palaeosol material supported by a bright red, muddy matrix that is composed of 54 % muscovite, 35 % quartz, 9 % haematite and 2 % albite (Table 1). Again, the overall composition of this lahar is compatible with a reworking of

material constrained to the weathered upper part of the underlying rhyolite, whereas its low TiO_2 content (0.43 wt %; Table 2) does not suggest any incorporation of weathered basaltic material from either below or above the rhyolite. Although this would be difficult to verify in a deposit that is composed of weathered material, there are no indications that this breccia was significantly weathered prior to tuff emplacement, which would suggest that this lahar is substantially younger than that at Section 3.

4.g. Lowermost tuff of the McGillivray Brook Formation

Although more cryptic than in the underlying volcanic rocks due to the fragmental nature of these volcanogenic sedimentary rocks, weathering is also apparent in the lowermost tuff of the McGillivray Brook Formation in the form of irregular areas of discolouration and textural contrasts. For the most part, each weathering event seems to extend beyond the thickness of individual tuff layers, and as a result, remnants of fresh tuff are rare. We have analysed the lowermost tuff layer at sections 1 and 3, and based on high loss on ignition (LOI) values and a lack of feldspars in both samples, we conclude that they were both thoroughly weathered following their deposition (Tables 1, 2). The weathered tuff is mainly composed of quartz (70–90 %), muscovite (6–18 %), haematite (4–8 %) and pyrophyllite (0–3 %; Table 1). As the Fe contents are excessively high for a felsic rock (2.82–7.08 wt % Fe_2O_3; Table 2), we conclude that the weathered tuff underwent eodiagenetic Fe-enrichment.

5. Intra-rhyolitic pedogenesis

The nearly complete breakdown of feldspars into secondary minerals, the near eradication of Na (Fig. 7b) and the absence of pedogenic calcite in the intra-rhyolitic palaeosol of the Dunn Point Formation altogether suggest that the latter evolved through most of its history under a warm and relatively humid climate. The significant thickness variability of the intra-rhyolitic weathering profile, from 0 to ~ 8.5 m over a small distance (Fig. 1b), is typical of weathering mantles in warm and humid environments because of the tendency of water to concentrate in low areas, which creates a positive feedback by attracting more water and therefore more weathering in those areas (Büdel, 1982; Petit, 1990; Gutierrez Elorza, 2006). The weathering mantle is therefore lenticular and separated by knobs of relatively fresh bedrock.

Based on strain calculations, Jutras, Quillan & LeForte (2009) estimated that the original thickness of the ~ 6 m thick A horizon at Section 1 was about three times thicker prior to burial compaction. Hence, the ~ 8.5 m thick profile at Section 1 is estimated to have been originally over 20 m thick. It is also inferred that the micaceous and chloritic fractions of the weathering profile are products of the diagenetic transformation of pedogenic clay minerals during deep burial. A more thorough evaluation of eodiagenetic and mesodiagenetic overprints is provided in subsequent sections.

Because rhyolite weathering at Section 3 was aborted by burial beneath a mafic flow, which itself had time to be thoroughly weathered before deposition of the lowermost tuff of the McGillivray Brook Formation, the truncated weathering profile at Section 3 probably evolved over a much shorter time than that at Section 1, thus potentially providing clues on early versus late pedogenic processes. In support of this, much greater soil maturity at Section 1 than at Section 3 is indicated by the presence of a well-developed B horizon in the former, which is absent in the latter.

One challenge in the comparison between the mature weathering profile at Section 1 and the immature profile at Section 3 is that the latter is part of the silica-enriched zone of Frenchman's Barn. This enrichment occurred shortly after rhyolitic emplacement along a tight network of vertical quartz veinlets that permeate the rhyolite in its entire thickness in that area, but that are truncated by the weathering profile.

5.a. Pedogenic Si-mobility

The pronounced Si-depletion that is observed in most of the intra-rhyolitic palaeosol profile at Section 1 (Fig. 7b) is to be expected in a warm and humid environment from the thorough breakdown of feldspars (Buxton, 1968). Its partial illuviation in the B and C horizons is more peculiar, but clearly pedogenic, as it is more than proportionally met by eluviation from the upper part of the profile (Fig. 7b). The lack of such enrichment in the immature profile at Section 3 (Fig. 7c) suggests that Si-illuviation only started occurring in the late stages of soil development. We interpret this enrichment to be partly related to the low porosity of the host rock, which would have caused some groundwater stagnancy at the base of the weathering profile, especially after the infiltration of a fair amount of secondary clay minerals had occurred.

The monsoonal climate that is inferred for the development of most of the underlying intra-basaltic palaeosol profiles (Jutras *et al.* 2012) is also compatible with the observed patterns of pedogenic Si-mobility in the intra-rhyolitic profile, as it would have provided the means to efficiently leach Si from the higher horizons during the wet seasons, whereas the dry seasons would have caused some of it to precipitate from gradual saturation in the stagnant aquifer above unweathered bedrock. This silica precipitation itself would have accentuated the situation, rendering the base of the profile even less permeable, and perhaps eventually preventing pedogenesis from evolving any deeper. In contrast with the underlying intra-basaltic palaeosols, in which periodic rises of the water-table during wet seasons are interpreted to have favoured the development of silcretes in the upper part of the profiles (Jutras *et al.* 2012), a lower water-table at the time of pedogenesis is inferred for the thicker and less dense rhyolite, which would not have favoured the peculiar upward

mobilization of Si that is observed in the former. Slightly lower Zr contents in the B and C horizons than in the host rock (Table 2), which we interpret to be the result of a dilution by pore-filling silica, suggests that no collapse occurred during deep burial in that part of the section owing to its silicic armature, again suggesting that this silica enrichment was pedogenic.

5.b. Pedogenic K-mobility

The distribution of K is among the most unexpected patterns in the weathering profile of the Ordovician rhyolite from the perspective of modern pedogenic environments (Fig. 7a). Because of the inherent acidity of today's warm and humid environments, greater K-leaching from the A horizon would be expected in the context of such a thorough breakdown of feldspars, and certainly no K-illuviation in the lowermost A subhorizon and into the B and C horizons. Such nearly proportional eluviation and illuviation patterns suggest a pedogenic origin for both the depletion and the enrichment rather than the works of subsequent diagenetic fluids, which is inferred for many pre-Silurian palaeosols (Gay & Grandstaff, 1980; Kimberley & Grandstaff, 1986; Zbinden *et al.* 1988; Feakes, Holland & Zbinden, 1989; Nesbitt & Young, 1989; Palmer, Philips & McCarthy, 1989; Krois, Stingl & Purtscheller, 1990; Rainbird, Nesbitt & Donaldson, 1990; Macfarlane & Holland, 1991; Fedo, Nesbitt & Young, 1995; Maynard *et al.* 1995; Rye & Holland, 2000; Mclennan, Simonetti & Goldstein, 2000; Panahi, Young, & Rainbird, 2000; Beukes *et al.* 2002; Yang, Holland & Rye, 2002; Utsunomiya *et al.* 2003; Jutras, Quillan & LeForte, 2009; Jutras *et al.* 2012).

This relative stability of K in the profile suggests that, despite the low base contents of the acidic host rock, soil water pH never evolved much below neutral. The inferred groundwater stagnancy at the base of the profile may have also contributed to the incorporation of K in pedogenic smectites at that level, again from gradual saturation during dry seasons. However, the observed K-enrichment in the C horizon of the immature palaeosol at Section 3 suggests that this illuviation started to occur quite early in the soil development history, prior to that of Si (Fig. 7c). It also suggests that, as the profile gradually deepened, the transition from K-eluviation to K-illuviation lowered accordingly, causing previously illuviated K to be remobilized again towards deeper levels.

As mentioned earlier, pedogenic patterns in the underlying intra-basaltic profiles as well as other clues from the clast contents of sedimentary rocks and from the diagenetic features of palaeosols suggest that early Palaeozoic times were prone to groundwater alkalinity due to the lack of a significant vegetation cover paired with lower rain acidity than in previous geological times (Jutras, Quillan & LeForte, 2009). The herein reported behaviour of K during the post-emplacement weathering of an Ordovician acidic host rock supports this conclusion.

5.c. Pedogenic Y-mobility

Yttrium-eluviation from the uppermost two A subhorizons is nearly proportionally met by illuviation in underlying horizons of the mature palaeosol at Section 1 (Fig. 7a), again suggesting pedogenic mobility. However, the eluvial section was originally three times thicker, whereas most of the illuvial section is silica-armoured and is inferred to have resisted compaction. Hence, a substantial amount of Y is interpreted to have left the system entirely.

In the shorter-lived palaeosol at Section 3, Y is leached throughout the thin profile (Fig. 7c). This suggests that this element was being leached in early stages of soil development, as is inferred for younger soils of warm and humid environments (Hill, Worden & Meighan, 2000). It also suggests that, contrary to K, it was not yet being illuviated into lower soil horizons during these early stages of pedogenesis. It can therefore be inferred that Y illuviation, which is nearly proportional to that of K in the lower ~ 3.5 m at Section 1 (Fig. 7a), only started occurring after the development of soil water stagnancy at the base of the profile due to clogging by silica.

5.d. Pedogenic Mg-mobility

Based on the proportion of Mg that was eluviated from the A horizon and illuviated into the B horizon (Fig. 7a), this element was no more mobile than Si during pedogenesis (Fig. 7b), which provides an additional piece of evidence that precludes low pH conditions. As Lawson *et al.* (2005) found that Mg can only be incongruently left behind above a pH of 8 during the weathering of silicates, its well-defined illuviation in the smectites of the B horizon (Figs 5, 7a) again suggests a high pH at that level, where stagnant groundwater above low-permeability rhyolite is inferred to have gradually concentrated its solution contents during dry seasons. The lack of Mg-enrichment in the C horizon suggests that its illuviation only occurred in the latest stages of weathering, when the C horizon was already clogged with silica, and when groundwater stagnation and pH at the base of the profile may have been highest.

5.e. Pedogenic Ti-mobility

Relatively constant TiO_2/Zr ratios through most of the profile at Section 1 (Fig. 7a) suggest that Ti was much more stable during rhyolite pedogenesis than during that of the well-developed intra-basaltic profiles below, which show well-defined Ti-cheluviation patterns (Jutras *et al.* 2012). The positive spike at −325 cm (Fig. 7a) is interpreted as an anomaly related to the low concentration of this element in the profile (Table 2), which can result in large variations from just the occasional presence of a large grain of anatase or ilmenite (observed as traces in thin-section; Figs 4, 5, 6). However, a moderate but convincing Ti-enrichment is observed in the B and C horizons (Fig. 7a), suggesting that this

element was not fully immobile. This enrichment is not clearly met by corresponding depletion in the overlying horizons (Fig. 7a), but, bearing in mind the limited resolution of such mass balance diagrams, Ti-leaching was possibly very weak in these thick horizons, which, as noted earlier, are estimated to have been about three times thicker prior to burial compaction. In contrast, the low Zr contents of the Si-enriched B and C horizons (Table 2) suggest slight inflation rather than collapse at that level. Hence, it can be estimated that the ~ 2 m thick area of moderate Ti-illuviation was fed by very faint eluviation from ~ 18 m of original soil profile.

Mobility of this typically immobile element remains to be explained, but Jutras *et al.* (2012) suggested that it may have been favoured by high pH and/or by the presence of chelates that were especially efficient at mobilizing this element, as cheluviation processes would best explain its proportional illuviation at the base of the intra-basaltic profiles of the Dunn Point Formation. The inferred high pH of Ordovician soil water is postulated to have harboured a very different population of bacteria, fungi and lichens, which would have therefore produced different varieties of chelates than those produced in today's acidity-prone environments (Jutras *et al.* 2012). Ti-chelation is suggested by the more substantial depletion of Ti that is observed at the top of the mature profile at Section 1 (Fig. 7a), where the production of chelates is concentrated. Ti-cheluviation is also inferred for the immature profile of Section 3 based on its significant enrichment in the C horizon, which is probably matched by leaching in the A horizon (Fig. 7c).

5.f. Pedogenic Al-mobility

There are two levels in the profile in which substantially lower Al_2O_3/Zr ratios suggest that significant Al-leaching has occurred (in the uppermost 2 m and between 4 and 6.5 m; Fig. 7b). The lack of a proportional lowering of SiO_2/Zr or TiO_2/Zr ratios (Fig. 7a and Table 2) does not suggest that these trends could be the artefacts of irregularities in Zr contents. Aluminium mobility in soils of warm and humid environments is controlled by the solubility of gibbsite, which is known to be least soluble at pH ~ 6.2, and less soluble than quartz between pH ~ 4.2 and ~ 9.5 (Blatt, Middleton & Murray, 1980). The alkalinity-prone Ordovician context and the behaviour of K and Mg in the same profile preclude a low pH setting for the Al-leaching. We therefore argue that these zones of Al-depletion must correspond to periods during which soil pH conditions may have ventured significantly above neutral near the base of the gradually deepening profile, where pH tends to be highest owing to the weathering of juvenile material, which systematically increases pH in common rocks (Keller, 1962; Schatz, 1963; Krug & Frink, 1983). In other words, these patterns may be inherited from different stages in the pedogenic history of the profile.

It is inferred that the soil would have developed a gradient of increasingly low groundwater pH conditions towards the surface, where low pH rain water was less buffered by mineral–water interactions, but in the absence of a significant vegetation cover, these lower pH conditions would have stayed well within the stability range of Al. Hence, it is inferred that each level of the profile was able to more or less maintain the Al concentration that it had acquired while in the juvenile zone, as each level would have subsequently evolved permanently under conditions in which Al is very stable. Abrupt changes in Al_2O_3/Zr ratios occur at −2, −4, −6.5 and −7.25 m, with intervals of relatively stable ratios in between (Fig. 7b).

6. Pedogenic versus eodiagenetic Fe-enrichments

One major challenge in palaeopedology is the necessity to discriminate physico-chemical changes that occurred during pedogenesis from those that occurred during subsequent diagenetic and metamorphic histories. In clay-dominated soil material, it can be argued that evenly distributed chemical leaching and enrichment can only occur prior to substantial burial compaction, which eventually makes the material impermeable.

Because excessive Fe-enrichment is observed in the entire weathering profile at Section 1, with none of the horizons showing a corresponding depletion (Fig. 7b), this enrichment cannot be entirely pedogenic. However, this enrichment is not associated with veins, but it is instead relatively well distributed in the authigenic phyllosilicate matrix that is interpreted to have developed from the diagenesis of pedogenic clays (Figs 5, 6). Fe-enrichment therefore occurred prior to deep burial compaction.

Iron-rich basalts are found below the rhyolite, but the lack of significant porosity in the latter makes the former an unlikely source for this Fe. Therefore, we consider the newly identified HFSE-rich basalt of the overlying McGillivray Brook Formation as a more likely source. As the contact between the tuff and the mature intra-rhyolitic palaeosol at Section 1 is non-erosive and seemingly conformable, we consider it unlikely that this basalt flow ever extended to that area. Moreover, as noted earlier, intra-rhyolitic pedogenesis was seemingly aborted early by burial under basalt at Section 3, but not at Section 1. As the tuff was also seemingly affected by this eodiagenetic Fe-enrichment (Tables 1, 2), it is inferred that lateral and vertical Fe-mobilization occurred in the reducing phreatic realm subsequent to tuff deposition, with Fe^{2+} lodging itself in smectite interlayers (Fig. 9c), and that partial oxidation occurred later (Fig. 9d).

Although the eodiagenetic Fe-enrichment was subsequent to pedogenesis, it was nonetheless favoured by greater permeability and a greater presence of accommodating smectites in the weathering profile than in the fresh rhyolite below, as suggested by the lack of such enrichment in the latter. It can be argued that eodiagenetic fluids were even less likely to infiltrate the silica-enriched Cq and Bgq horizons. Some reduced Fe was

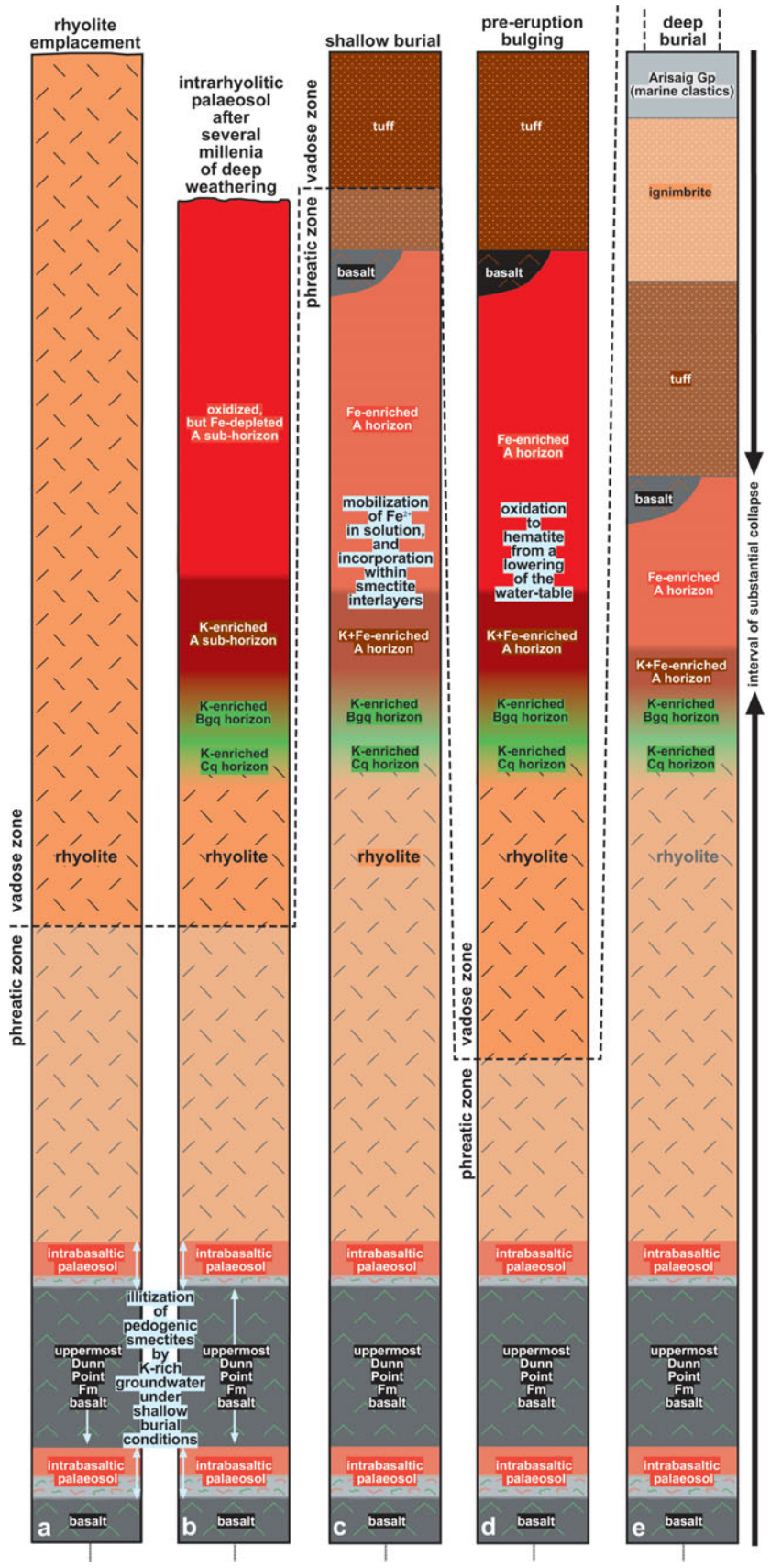

Figure 9. (Colour online) Pedogenic and diagenetic model for the intra-rhyolitic palaeosol of the Middle to Upper Ordovician Dunn Point Formation. (a) Development of a low water-table following the emplacement of thick rhyolite, and beginning of an illitization of pedogenic smectites in the underlying intra-basaltic palaeosols by K-rich groundwaters under shallow burial conditions, as discussed in Jutras *et al.* (2012). (b) Development of a thick and mature palaeosol after several millennia of deep weathering. At this stage, the A horizon is inferred to have been oxidized and moderately depleted in Fe, whereas the B horizon would have been already enriched in this element. (c) Eodiagenetic Fe-enrichment of A horizon smectites in reducing phreatic conditions following the emplacement of

maintained as 'green rust' in the Bgq horizon, which may have developed from groundwater stagnation at the base of the profile during pedogenesis, suggesting that this horizon was not affected by the subsequent, post-pedogenic oxidation event that affected the A horizon. This observation suggests that the silica-clogged Cq and Bgq horizons acted as a chemically closed system in subsequent diagenetic environments and that their chemical contents are proportional to those at the time of pedogenesis. Hence, as these horizons are nonetheless substantially enriched in Fe (Figs 5, 7b), it can be inferred that this element was not immobile at the time of soil formation and that pedogenic Fe-eluviation proportional to its observed illuviation in the B and C horizons (Figs 7b, 9b) may have been obscured by substantial additions of Fe in the A horizon after burial (Fig. 8c). Such Fe-cheluviation patterns are observed in the underlying intra-basaltic palaeosols, which Jutras *et al.* (2012) hypothesized as having been related to a high productivity of siderophores in the primitive Ordovician vegetation cover.

Whereas pedogenic Fe is evenly disseminated in the phyllosilicate matrix of the silica-armoured B horizon (Fig. 5), eodiagenetic Fe in the A horizon is instead concentrated in discrete areas (now in chamosite) from which K was displaced into the immediate surroundings (Fig. 6). This minor segregation suggests that minor, shallow burial compaction had already occurred in the A horizon by the time this eodiagenetic enrichment took place. Because the contaminated uppermost part of the A horizon may have seen much of its clay contents convert to micas during the emplacement of the overlying tuff, it was able to accommodate less Fe^{2+} than the rest of this horizon (Fig. 7b) during the subsequent circulation of eodiagenetic fluids.

The oxidation event that followed eodiagenetic Fe-enrichment resulted in the formation of specks of haematite that displaced some of the remaining *in situ* K into the immediate surroundings (Fig. 6). High Ti contents in this post-pedogenic haematite (Fig. 6) suggest that this element was present as a minor exchangeable cation within the smectites and was leached from the clay matrix during the formation of haematite. This partial oxidation to haematite probably occurred prior to the basal Silurian transgression, which from then onwards kept the system under sea water until well into the Late Silurian, by which time the palaeosols would have been buried below nearly 1 km of strata (Boucot *et al.* 1974). In the context of a stratovolcano, the most probable scenario for this oxidation event would involve the substantial bulging and associated lowering of the water-table that must have preceded the explosive *nuée ardente* that left thick ignimbrite above the tuff (Fig. 9d).

7. Mesodiagenetic overprints

Based on the discussion above, we interpret the pre-eodiagenetic composition of the B horizon of the mature palaeosol at Section 1 as a mixture of cryptocrystalline quartz and K- and Fe-rich smectites, and the A horizon as a mixture of gibbsite, kaolinite, relatively K-rich smectites and minor haematite (Fig. 9b). As noted earlier, smectites of the latter horizon were subsequently enriched in eodiagenetic Fe (Fig. 9c), which was in part oxidized to haematite later in the eodiagenetic history (Fig. 9d).

Whereas gibbsite and haematite would have persisted during deep burial, the kaolinite and K-rich smectites of the A horizon evolved into closely interstratified pyrophyllite and muscovite, whereas the smectites that were enriched in eodiagenetic Fe evolved into discrete areas of chamosite (Table 1; Fig. 6). In the silica-enclosed Bgq horizon, smectites with better disseminated K and pedogenic Fe evolved into closely interstratified muscovite and biotite (Table 1; Fig. 5). In the process, some Fe was leached from perhaps more permeable areas of the A horizon, probably during dewatering in poorly consolidated early stages of deep burial. This left some sharply defined white areas from which Fe was seemingly even leached out of ilmenite to form specks of anatase (i.e. leucoxene) (Fig. 6). This late diagenetic leaching seemingly only affected Fe among major elements, as the concentrations of K and Mg are undisturbed in the Fe-free white spots (Fig. 6). Again, because these elements are highly soluble in the acidic range, this suggests that the early mesodiagenetic environment in which Fe is inferred to have been partially leached also occurred at high pH. This corroborates the suggestion of Jutras, Quillan & LeForte (2009), according to whom pre-Silurian deep burial environments must have also been prone to developing higher pH than those of subsequent geological times because of the paucity of organic matter in the mostly coal-free sedimentary rocks of the pre-Silurian continental crust.

8. Record of palaeoclimate fluctuations

Two types of palaeosols were identified in the succession of weathered basalt flows that underlies the rhyolite, which Jutras *et al.* (2012) attributed to climatic fluctuations at the scale of Croll–Milankovitch cycles. However, as noted earlier, the substantially greater thickness of the intra-rhyolitic palaeosol and the more weathering-resistant nature of its host rock suggest that it developed over a much longer period of time and that such cyclicity would most likely have been recorded within the single profile. Because Al is only mobile under extreme environmental conditions, which, in the absence of vascular plants, could only develop in the

basalt and tuff above the intra-rhyolitic palaeosol, which caused the water-table to rise above the weathering profile. (d) Temporary lowering of the water-table and partial oxidation of the A horizon, possibly during the bulging that must have preceded the eruption of *nuées ardentes* above the tuff.

juvenile zone of weathering and never again after this zone had moved to lower levels, these climatic fluctuations are best recorded by variations in Al_2O_3/Zr ratios.

8.a. Stage 1

Low Al_2O_3/Zr ratios in the uppermost ~2 m at Section 1 (Fig. 7b) may have resulted from the development of high soil water pH in early stages of soil development because of mineral–water interactions, a lack of significant organic acid inputs and a tendency towards groundwater stagnation in the weathering profile due to the low permeability of the rhyolitic host rock (Fig. 10a). As Al-contamination from the overlying tuff is unlikely, gradually decreasing Al_2O_3/Zr ratios downwards from the surface in the uppermost 1.5 m of the palaeosol (Fig. 7b) may reflect gradual aggravation of the high pH conditions in the juvenile zone as the latter was progressing further below the main source of organic acids (Fig. 10b), which would have been at the surface in early Palaeozoic times due to the absence of vascular plants. The conclusion that some Al-leaching occurred in early stages of soil development is supported by evidence for such leaching in the immature profile of Section 3 (Fig. 7c).

Because the base of the profiles was not yet clogged with silica at this stage, the mobilized Al may have been lost to the groundwater system, thus leaving the profiles entirely (Fig. 10a, b). However, in the case of K, because its solubility decreases as pH increases, this element must have been incorporated in smectites at the base of the profile at all stages of its evolution, as suggested by the significant K-enrichment that is observed at the base of the immature profile of Section 3 (Fig. 7a), only to be remobilized under lower pH conditions as the juvenile zone migrated to lower levels in the longer lasting case of Section 1.

Some minor Ti-cheluviation is observed at Section 3 (Fig. 7c), and Fe is also inferred to have experienced minor cheluviation in the early stages of pedogenesis, although this would have been masked by subsequent eodiagenetic enrichment. All other studied elements (Na, Y, Mg and Si) are inferred to have undergone net leaching out of the system in early stages of pedogenesis (Fig. 10a, b) based on data from Section 3 (Fig. 7c).

8.b. Stage 2

The pronounced increase in Al_2O_3/Zr ratios that is observed between the −1.5 to −2 m interval at Section 1 (Fig. 7b) is interpreted to reflect climate change towards conditions in which Al was relatively stable in the entire profile, as reflected by Al_2O_3/Zr ratios that are more or less equal to that of the host rock in the underlying −2 to −4 m interval (Fig. 7b). Hence, we interpret that when the juvenile base of the weathering profile was deepening down into the level of this interval, soil water pH was generally not far from neutral anywhere in the profile (Fig. 10c, d). In this context, the signature of more extreme soil water pH conditions inherited from Stage 1 would have remained intact, higher in the profile, as Al could neither be removed nor added in near-neutral soil water pH conditions. However, leaching of Na, Si, Mg and K probably kept occurring in those conditions, some of which may have illuviated lower down (Fig. 10c), but only to be leached again at subsequent stages of soil development (Fig. 10d, e, f).

8.c. Stage 3

The abrupt lowering of Al_2O_3/Zr ratios at −4 m in Section 1 (Fig. 7b) is again interpreted as reflecting climate change when this level corresponded to the juvenile zone of weathering, marking a return to conditions in which Al was unstable in that zone. A substantially greater thickness of the lower interval of low Al_2O_3/Zr ratios (Stage 3) compared to that of the interval with stable Al_2O_3/Zr ratios (Stage 2) does not necessarily reflect a longer climate cycle, as the rates of profile deepening may have differed greatly from one climate setting to the next. Moreover, reworking of the base of the zone of stable Al_2O_3/Zr ratios that was inherited from Stage 2 may have occurred in the upper part of the juvenile zone of weathering after it returned to high pH conditions in which Al was once again unstable (Fig. 10e). In other words, the interval corresponding to Stage 2 (Fig. 7b) may have been originally thicker and subsequently scavenged by processes that took place during Stage 3. To this effect, we interpret that the interval in which Al was actively being leached may have been thicker at Stage 3 than at Stage 1 because of the less steep pH gradient that is inferred for this phase of soil development, as the juvenile zone of weathering was by then much further from organic and rain acid inputs from the surface (Fig. 10e).

The second cycle of Al-mobility (Stage 3) involves a greater cumulative portion of the section than the previous (Stage 1) (Fig. 7b) and therefore must have lasted longer. We argue that the early part of Stage 3 must have been similar to the pedogenic dynamics of Stage 1 (Fig. 10e), but as the profile matured, substantial clogging by secondary clay minerals may have increased groundwater stagnation at the base of the profile, which in turn must have caused silica to start precipitating, thus aggravating the clogging (Figs 7b, 10f). This increased stagnation at the base of the profile may have also caused the illuviation of Y and Ti, which extends into the Cq horizon (Figs 7a, 10f), and eventually that of Mg and Al, which is limited to the Bgq horizon (Figs 7b, 10g).

The eventual incapacity of groundwater to penetrate the silica-enriched Cq horizon (−7.25 to −8.5 m interval) may have prevented the soil from deepening any further and may have prevented this horizon from being thoroughly weathered. Hence, this immature horizon may have become what it is long before the abortion of pedogenesis by burial under tuff. This impermeability must have gradually extended into the B horizon from

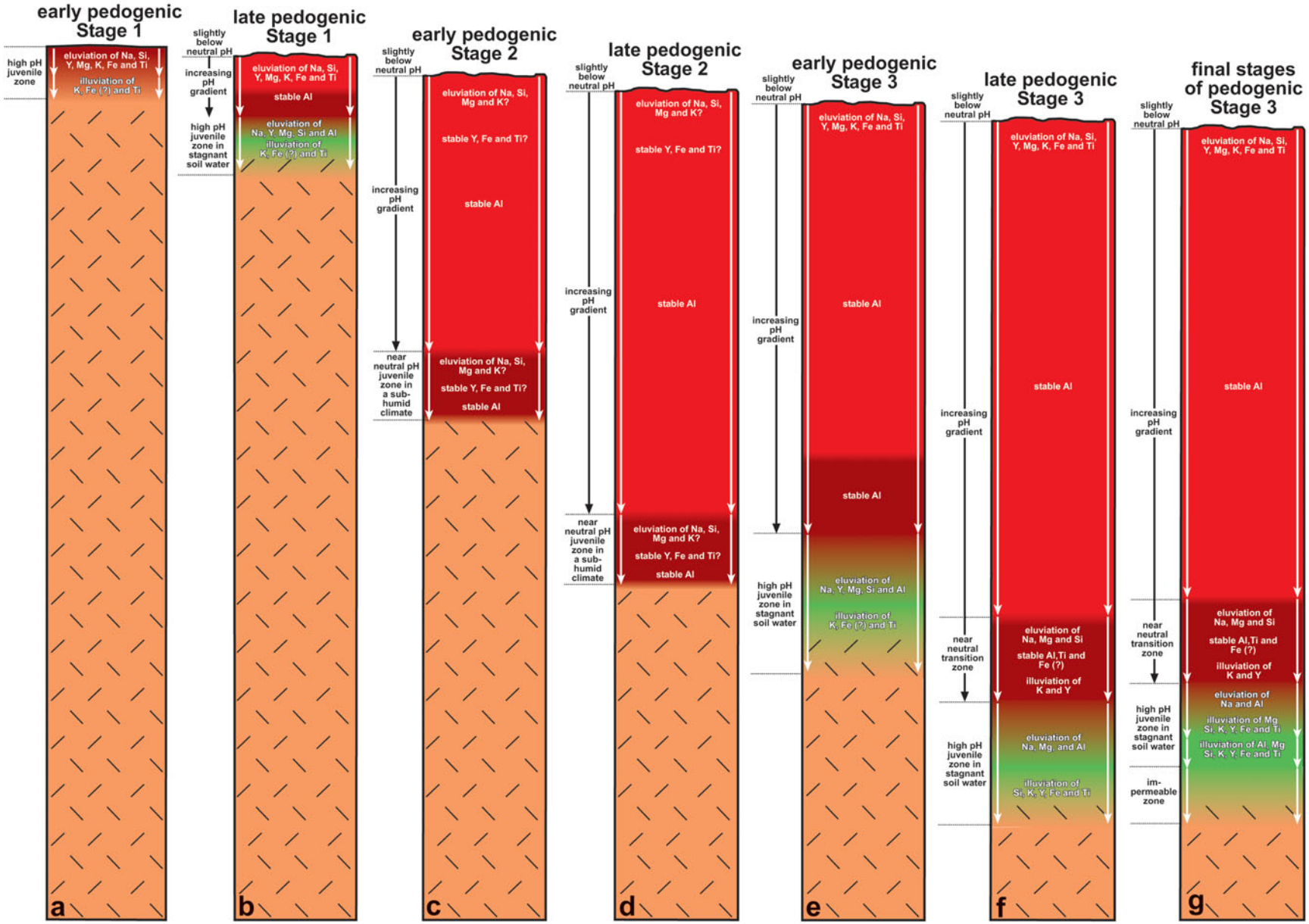

Figure 10. (Colour online) (a–g) Detailed pedogenic model for the intra-rhyolitic palaeosol at Section 1 (see text for discussion).

the continuation of silica precipitation, as suggested by the observation that the resulting Bgq horizon was not oxidized during the subsequent eodiagenetic events that enriched the rest of the profile with haematite.

8.d. Types of climate involved

As noted earlier, two types of palaeosols were identified by Jutras *et al.* (2012) in the basalt succession that underlies the rhyolite. Most correspond to a 'red-silcrete-bearing facies' that shows evidence of having evolved under a monsoonal climate (i.e. with a well-defined rainy season followed by a prolonged dry season; Jutras *et al.* 2012). However, other profiles do not include a red silcrete and seem to have evolved without a well-defined rainy season, and in overall drier conditions, although not dry enough to have prevented a fairly efficient destruction of feldspars (i.e. a warm and sub-humid climate; Jutras *et al.* 2012). If the same types of climate alternated during rhyolite pedogenesis, it is argued that, although soil water would have been less often buffered by low pH rain water in a drier climate, Al was more likely to be mobilized in a monsoonal climate, when weathering was more efficient, and when the base of the weathering profile above low-permeability rhyolite was remaining water-saturated long enough to develop a sufficiently high pH. Hence, stages 1 and 3 would possibly correspond to the climate setting that produced the red-silcrete-bearing facies, and Stage 2 would correspond to that of the non-silcrete-bearing facies.

8.e. Constraints on the climatic history of the faulted intra-basaltic palaeosol above rhyolite at sections 3 and 4

As the truncated intra-rhyolitic profile at Section 3 does not show evidence of having evolved beyond Stage 1, and as the intervening lahar does not show evidence of having been exposed to prolonged weathering, it can be inferred that the overlying basalt was weathered through all of stages 2 and 3, and possibly the end of Stage 1. Although the lack of a full section of this intra-basaltic weathering profile limits its study, available data are compatible with this profile being a hybrid between the two types of palaeosols that are found in the succession below the rhyolite. Some Si-leaching would have occurred during the inferred sub-humid conditions of Stage 2, but as the volcano was by then bimodal, the lack of a high water-table would have not subsequently allowed the upward migration of silica that is inferred to have occurred in the red-silcrete-bearing facies of the underlying mafic succession (Jutras *et al.* 2012) in a similar climatic setting to that of Stage 3. Apart from the lack of Si-enrichment, the depletion in Al, Fe and Ti that is observed at the top of the intra-basaltic palaeosol in the McGillivray Brook Formation at Section 3, in increasing order of depletion (Fig. 7d), is similar to that observed in the A horizon of the red-silcrete-bearing palaeosols in the underlying Dunn Point Formation (Jutras *et al.* 2012).

9. Conclusions

Well-defined eluviation and cheluviation patterns of several elements (Si, K, Mg, Y and, to a lesser degree, Ti and Al) in the intra-rhyolitic palaeosol that tops the Middle to Upper Ordovician Dunn Point Formation indicate that much of its pedogenic signature was preserved despite the overprint of its subsequent diagenetic history. This thick palaeosol seemingly evolved under the same two types of warm climates as the intra-basaltic palaeosols below (monsoonal and sub-humid; Jutras *et al.* 2012), but long enough to go through at least two episodes of significant climate change, something that is not observed in the much shorter intra-basaltic weathering events that marked the base of the succession. In the early and late stages of intra-rhyolitic weathering (stages 1 and 3), the prevailing hot and relatively humid climate was not only efficient at breaking down feldspars and mobilizing Si, but also at mobilizing Al, Y, Fe and some Ti, suggesting extreme conditions of weathering (Fig. 10a, b). As K was less mobile than Si, being less eluviated from the upper part of the profile and better illuviated at the base of the profile, it can be inferred that these extreme conditions were in the high pH range, as K is very unstable in low pH environments. Owing to the very poor K contents of their host rocks, such K-cheluviation patterns were not observed in the intra-basaltic profiles (Jutras *et al.* 2012 and this study) as they would have been masked by subsequent eodiagenetic K-enrichment, which is inferred to have been sourced from the thick rhyolite (Fig. 9a, b).

The combination of relatively humid conditions and high pH soil water cannot be achieved in modern pedogenic environments because of the significantly acidifying influence of vascular plants, and no modern analogue therefore exists for such a setting. Just as in the case of the intra-basaltic profiles, the mobility of Fe and Ti in the intra-rhyolitic profile is tentatively explained by the presence of chelates that were especially efficient at mobilizing these elements and that may have been produced by bacteria, algae and lichen that differed greatly from those of modern environments as they were thriving in a high pH humid environment that is now virtually 'extinct' (Jutras *et al.* 2012). In the case of Al, its mobility can be best explained by the development of very high pH (above 8) in the juvenile base of the weathering profile, where greatest pH values can be attained owing to the concentrated weathering of primary minerals.

Titanium was not nearly as mobile in the intra-rhyolitic profile as it was in its intra-basaltic counterparts (Jutras *et al.* 2012 and this study), which may be related to the lower base contents of acid rocks. Moreover, the silica enrichment that occurred in the upper part of the intra-basaltic profiles in the Dunn Point Formation (Jutras *et al.* 2012) is not observed in the intra-rhyolitic palaeosol, nor in the overlying intra-basaltic palaeosol of the McGillivray Brook Formation, possibly owing to a lower water-table during formation

of the latter two profiles, which can be inferred owing to the greater thickness and lower density of the felsic rocks. Despite these minor differences, the same type of monsoonal climate is inferred to have affected both types of host rock at Arisaig, allowing element saturation and high pH conditions to develop during the dry season at the top of the water-table, in the case of the intra-basaltic profiles of the Dunn Point Formation (Jutras *et al.* 2012), or, in the case of the intra-rhyolitic palaeosol, in trapped soil water above the low-permeability base of the profile.

Because of the increased distance between the juvenile zone of weathering and acid inputs from rain and organic activity at the surface, and because of a gradual increase in soil water stagnation at the base of the profile during the dry season due to gradual clogging by clay minerals, more elements were illuviated in the lower horizons during Stage 3 (Y, K, Si, Mg, Fe, Ti and Al; Fig. 7a, b) than during the shorter-lived Stage 1 (K, Ti and maybe Fe; Fig. 7c). In the case of Fe, Mg and Al, which are only enriched above the C horizon at Section 1, it seems that silica-clogging was a prerequisite to generate sufficient soil water stagnation at the base of the profile for these elements to be retained as exchangeable cations in smectites.

A ~ 2 m thick interval of Al stability in the rhyolite palaeosol (Stage 2 on Fig. 7b) is interpreted to reflect a time of less extreme groundwater conditions when this interval corresponded to the juvenile zone of weathering (Fig. 10c, d). Not much else can be said about the climate corresponding to this interval in the intra-rhyolitic profile, as its associated Al_2O_3/Zr ratios are the only signature that survived the subsequent return to more extreme weathering conditions (Stage 3). However, the climate at Stage 2 can be inferred to have been similar to the less aggressive climate that left palaeosols with no silcretes, more carbonate and a less thorough leaching of soluble cations in the intra-basaltic succession below, which Jutras *et al.* (2012) associated with a sub-humid climate from colder and more arid orbital cycles.

In conclusion, although the chances of preservation are very slight owing to potential reworking by subsequent pedogenic and diagenetic events, climatic fluctuations may in some cases be recorded in thick palaeosols that have evolved over a very long period of time. However, the preserved signatures can only come from elements that are only mobile in very specific conditions, such as Al. Although this greatly limits the use of single palaeosols as recorders of past climate change, long-lasting weathering profiles can still occasionally provide signatures of events of extreme environmental conditions in the geological record.

Acknowledgements. We wish to thank R. Corney for the making of thin-sections, M. Préda for providing X-ray diffraction analyses, and X. Yang for providing X-ray fluorescence analyses and support with the SEM. We also wish to thank P. Leat and two anonymous reviewers for their constructive comments on this manuscript. This project was funded by a FGSR University Grant in Aid of Research, #200292-5760-83540-9999.

References

ANDA, M., SHAMSUDDIN, J., CHE FAUZIAH, I. & SYED OMAR, S. R. 2008. Mineralogy and factors controlling charge development of three Oxisols developed from different parent materials. *Geoderma* **143**, 153–67.

ANDERSON, S. P., DIETRICH, W. E. & BRIMHALL, G. H., JR. 2002. Weathering profiles, mass-balance analysis, and rates of solute loss: linkages between weathering and erosion in a small, steep catchment. *Geological Society of America Bulletin* **114**, 1143–58.

BASU, A. 1981. Weathering before the advent of land plants; evidence from unaltered detrital K-feldspars in Cambrian-Ordovician arenites. *Geology* **9**, 132–3.

BEUKES, N. J., DORLAND, H., GUTZMER, J., NEDACHI, M. & OHMOTO, H. 2002. Tropical laterites, life on land, and the history of atmospheric oxygen in the Palaeoproterozoic. *Geology* **30**, 491–94.

BLATT, H., MIDDLETON, G. & MURRAY, R. 1980. *Origin of Sedimentary Rocks*, 2nd ed. Englewood Cliffs: Prentice-Hall, 782 pp.

BRIMHALL, G. H., JR., CHADWICK, O. A., LEWIS, C. J., COMPSTON, W., WILLIAMS, I. S., DANTI, K. J., DIETRICH, W. E., POWER, M. E., HENDRICKS, D. & BRATT, J. 1992. Deformational mass transport and invasive processes in soil evolution. *Science* **255**, 695–702.

BOUCOT, A. J., DEWEY, J. F., DINELEY, D. L., FLETCHER, R., FYSON, W. K., GRIFFIN, J. G., HICKOX, C. F., MCKERROW, W. S. & ZIEGLER, A. M. 1974. *Geology of the Arisaig area, Antigonish County, Nova Scotia*. Geological Society of America, Special Paper no. 139.

BÜDEL, J. 1982 (translated by L. Fischer & D. Busche). *Climatic Geomorphology*. Princeton University Press, 443 pp.

BUGGLE, B., HAMBACH, U., GERASIMENKO, N., GLASER, B., MARKOVIĆ, S. B. & ZÖLLER, L. 2009. Stratigraphy and spatial and temporal paleoclimatic trends in East European loess paleosol sequences. *Quaternary International* **196**, 86–106.

BUGGLE, B., HAMBACH, U., KEHL, M., ZÖLLER, L., MARKOVIĆ, S. B. & GLASER, B. 2013. The progressive evolution of a continental climate in SE-Central European lowlands during the Middle Pleistocene recorded in loess paleosol sequences. *Geology* **41**, 771–4.

BUGGLE, B., HAMBACH, U., MÜLLER, K., ZÖLLER, L., MARKOVIĆ, S. B. & GLASER, B. 2014. Iron mineralogical proxies and Quaternary climate change in SE-European loess–paleosol sequences. *Catena* **117**, 4–22.

BUXTON, B. P. 1968. Measure of the degree of chemical weathering of rocks. *Journal of Geology* **76**, 518–27.

CHAPUIS-LARDY, L., BROSSARD, M. & QUIQUAMPOIX, H. 2001. Assessing organic phosphorus status of Cerrado oxisols (Brazil) using 31P-NMR spectroscopy and phosphomonoesterase activity measurement. *Canadian Journal of Soil Science* **81**, 591–601.

FEAKES, C. R., HOLLAND, H. D. & ZBINDEN, E. A. 1989. Ordovician palaeosols at Arisaig, Nova Scotia, and the evolution of the atmosphere. *Catena Supplement* **16**, 207–32.

FEDO, C. M., NESBITT, H. W. & YOUNG, G. M. 1995. Unraveling the effects of potassium metasomatism in sedimentary rocks and palaeosols, with implications for palaeoweathering conditions and provenance. *Geology* **23**, 921–4.

GAY, A. L. & GRANDSTAFF, D. E. 1980. Chemistry and mineralogy of Precambrian palaeosols at Elliot Lake, Ontario, Canada. *Precambrian Research* **12**, 349–73.

GUTIERREZ ELORZA, M. 2006. *Climatic Geomorphology*. Developments in Earth Surface Processes, Vol. 8. Elsevier Science, 774 pp.

HAMILTON, M. A. & MURPHY, J. B. 2004. Tectonic significance of a Llanvirn age for the Dunn Point volcanic rocks, Avalon terranes, Nova Scotia, Canada: implications for the evolution of the Iapetus and Rheic oceans. *Tectonophysics* **379**, 199–209.

HILL, I. G., WORDEN, R. H. & MEIGHAN, I. G. 2000. Yttrium; the immobility-mobility transition during basaltic weathering. *Geology* **28**, 923–6.

HODSON, M. E. 2002. Experimental evidence for mobility of Zr and other trace elements in soils. *Geochimica et Cosmochimica Acta* **66**, 819–28.

ISMAIL, H., SHAMSHUDDIN, J. & SYED OMAR, S. R. 1993. Alleviation of soil acidity in Ultisol and Oxisol for corn growth. *Plant and Soil* **151**, 55–65.

JUTRAS, P., HANLEY, J. J., QUILLAN, R. S. & LEFORTE, M. J. 2012. Intra-basaltic soil formation, sedimentary reworking and eodiagenetic K-enrichment in the Middle to Upper Ordovician Dunn Point Formation of eastern Canada: a rare window into early Paleozoic surface and near-surface conditions. *Geological Magazine* **149**, 798–818.

JUTRAS, P., QUILLAN, R. S. & LEFORTE, M. J. 2009. Evidence from Middle Ordovician palaeosols for the predominance of alkaline groundwater at the dawn of land plant radiation. *Geology* **37**, 91–4.

KASTING, J. F. 1993. Earth's early atmosphere. *Science* **259**, 920–6.

KELLER, W. D. 1962. *The Principles of Chemical Weathering*. Lucas Bros. Publishers, 111 pp.

KIMBERLEY, M. M. & GRANDSTAFF, D. E. 1986. Profiles of elemental concentrations in the Precambrian atmosphere. *Precambrian Research* **34**, 205–29.

KLEINERT, K. & STRECKER, M. R. 2001. Climate change in response to orographic barrier uplift: paleosol and stable isotope evidence from the late Neogene Santa María basin, northwestern Argentina. *Geological Society of America Bulletin* **113**, 728–42.

KRAUS, M. J. 1999. Paleosols in clastic sedimentary rocks: their geologic applications. *Earth-Science Reviews* **47**, 41–70.

KROIS, P., STINGL, V. & PURTSCHELLER, F. 1990. Metamorphosed weathering horizon from the Oetztal-Stubai crystalline complex (Eastern Alps, Austria). *Geology* **18**, 1095–8.

KRUG, E. C. & FRINK, C. R. 1983. Acid rain on acid soil; a new perspective. *Science* **217**, 520–5.

LAWSON, R. T., COMARMOND, M.-C. J., RAJARATNAM, G. & BROWN, P. L. 2005. The kinetics of the dissolution of chlorite as a function of pH and at 25 °C. *Geochimica et Cosmochimica Acta* **69**, 1687–99.

MACFARLANE, A. W. & HOLLAND, H. D. 1991. The timing of alkali metasomatism in palaeosols. *Canadian Mineralogist* **29**, 1043–50.

MAYNARD, J. B., SUTTON, S. J., ROBB, L. J., FERRAZ, M. F. & MEYER, F. M. 1995. A Palaeosol developed on hydrothermally altered granite from the hinterland of the Witwatersrand Basin; characteristics of a source of basin fill. *Journal of Geology* **103**, 357–77.

MCLENNAN, S. M., SIMONETTI, A. & GOLDSTEIN, S. L. 2000. Nb and Pb isotopic evidence for provenance and post depositional alteration of the Palaeoproterozoic Huronian Supergroup, Canada. *Precambrian Research* **102**, 263–78.

METZGERA, C. A. & RETALLACK, G. J. 2010. Paleosol record of Neogene climate change in the Australian outback. *Australian Journal of Earth Sciences* **57**, 871–85.

MURPHY, J. B., DOSTAL, J. & KEPPIE, J. D. 2008. Neoproterozoic–Early Devonian magmatism in the Antigonish Highlands, Avalon terrane, Nova Scotia: tracking the evolution of the mantle and crustal sources during the evolution of the Rheic Ocean. *Tectonophysics* **461**, 181–201.

MURPHY, J. B., HAMILTON, M. A. & LEBLANC, B. 2012. Tectonic significance of Late Ordovician silicic magmatism, Avalon terrane, northern Antigonish Highlands, Nova Scotia. *Canadian Journal of Earth Sciences* **49**, 346–58.

MURPHY, J. B., KEPPIE, J. D. & HYNES, A. J. 1991. Geology of the Antigonish Highlands. *Geological Survey of Canada Paper* **89–10**, 114 pp.

NESBITT, H. W. & YOUNG, G. M. 1989. Formation and diagenesis of weathering profiles. *Journal of Geology* **97**, 129–47.

OKULITCH, A. V. 2004. *Geological Time Chart, 2004*. Geological Survey of Canada Open-File 3040 (National Earth Science Series, Geological Atlas)–Revision.

OLIVEIRA, F. H. T., NOVAISA, R. F., SMYTHB, T. J. & NEVESA, J. C. L. 2000. Aluminum diffusion in Oxisols as influenced by soil water matric potential, pH, lime, gypsum, potassium chloride, and calcium phosphate. *Communications in Soil Science and Plant Analysis* **31**, 2523–33.

PALMER, J. A., PHILIPS, G. N., & MCCARTHY, T. S. 1989. Palaeosols and their relevance to Precambrian atmospheric composition. *Journal of Geology*, **97**, 77–92.

PANAHI, A., YOUNG, G. M. & RAINBIRD, R. H. 2000. Behavior of major and trace elements (including REE) during Palaeoproterozoic pedogenesis and diagenetic alteration of an Archean granite near Ville Marie, Quebec, Canada. *Geochimica et Cosmochimica Acta* **64**, 2199–20.

PERYAM, T. C., DORSEY, R. J. & BINDEMAN, I. 2011. Plio-Pleistocene climate change and timing of Peninsular Ranges uplift in southern California: evidence from paleosols and stable isotopes in the Fish Creek–Vallecito basin. *Palaeogeography, Palaeoclimatology, Palaeoecology* **305**, 65–74.

PETIT, M. 1990. *Géographie Physique Tropicale; Approches aux Études de Milieu, Morphogénèse, Paysage*. Karthala-ACCT, 351 pp.

RAINBIRD, R. H., NESBITT, H. W. & DONALDSON, J. A. 1990. Formation and diagenesis of a sub-Huronian saprolith: comparison with a modern weathering profile. *Journal of Geology* **98**, 801–22.

RYE, R. & HOLLAND, H. D. 2000. Geology and geochemistry of palaeosols developed on the Hekpoort basalt, Pretoria Group, South Africa. *American Journal of Science* **300**, 85–141.

SALTZMAN, M. R. & YOUNG, S. A. 2005. Long-lived glaciation in the Late Ordovician? Isotopic and sequence-stratigraphic evidence from western Laurentia. *Geology* **33**, 109–12.

SCHAEFER, C. E. G. R., FABRIS, J. D. & KER, J. C. 2008. Minerals in the clay fraction of Brazilian Latosols (Oxisols): a review. *Clay Minerals* **43**, 137–54.

SCHATZ, A. 1963. Soil microorganisms and soil chelation: the pedogenic action of lichens and lichen acids. *Agricultural Food Chemistry* **11**, 112–8.

SHAMSHUDDIN, J. & ANDA, M. 2012. Enhancing the productivity of Ultisols and Oxisols in Malaysia using basalt and/or compost. *Pedologist* **55**, 382–91.

SOIL SURVEY STAFF., 2010. *Keys to Soil Taxonomy*, 11th ed. Washington, D.C.: USDA–Natural Resources Conservation Service, 338 pp.

UTSUNOMIYA, S., MURAKAMI, T., NAKADA, M. L. & KASAMA, T. 2003. Iron oxidation state of a 2.45-Byr-old palaeosol developed on mafic volcanics. *Geochimica et Cosmochimica Acta* **67**, 213–21.

VAN DER VOO, R. & JOHNSON, R. J. E. 1985. Palaeomagnetism of the Dunn Point Formation (Nova Scotia): high palaeolatitudes for the Avalon terrane in the Late Ordovician. *Geophysical Research Letters* **12**, 337–40.

WALKER, J. D. & GEISSMAN, J. W. (compilers) 2009. *Geologic Time Scale*. The Geological Society of America.

WEAVER, C. E. 1989. *Clays, Muds, and Shales*. Developments in Sedimentology Vol. 44. Burlington: Elsevier, 819 pp.

WINCHESTER, J. A. & FLOYD, P. A. 1977. Geochemical discrimination of different magma series and their differentiation products using immobile elements. *Chemical Geology* **20**, 325–3.

YANG, W., HOLLAND, H. D. & RYE, B. 2002. Evidence for low or no oxygen in the late Archean atmosphere from the ~ 2.76 Ga Mt. Roe #2 palaeosol, Western Australia: Part 3. *Geochimica et Cosmochimica Acta* **66**, 3707–81.

ZBINDEN, E. A., HOLLAND, H. D., FEAKES, C. R. & DOBOS, S. K. 1988. The Sturgeon Falls palaeosol and the composition of the atmosphere 1.1 Ga BP. *Precambrian Research* **42**, 141–63.